MINIMALLY INVASIVE ASSESSMENT OF LYMPHATIC PUMPING PRESSURE USING FUNCTIONAL NEAR INFRARED IMAGING

A Masters Thesis
Presented to
The Academic Faculty

by

Ryan E. Akin

In Partial Fulfillment
of the Requirements for the Degree
Masters of Science in the
School of Mechanical Engineering

Georgia Institute of Technology
May 2013

MINIMALLY INVASIVE ASSESSMENT OF LYMPHATIC PUMPING PRESSURE USING FUNCTIONAL NEAR INFRARED IMAGING

Approved by:

Dr. J. Brandon Dixon, Advisor
School of Biomedical Engineering
Georgia Institute of Technology

Dr. David N. Ku
School of Mechanical Engineering
Georgia Institute of Technology

Dr. Rudolph L. Gleason
School of Mechanical Engineering
Georgia Institute of Technology

Date Approved: January 8, 2013

To the glory of God, the Creator of the lymphatic system, Author of all knowledge, and Provider of my opportunity to pursue a Masters thesis.

ACKNOWLEDGEMENTS

I would like to thank Dr. J. Brandon Dixon, the leader of the Laboratory of Lymphatic Biology and Bioengineering at the Georgia Institute of Technology and my advisor throughout graduate school and the scientific discovery process. He has generously given of his time, ideas, efforts, and funding to ensure quality work on my behalf. I am incredibly grateful to several of my fellow lab members (Jeff Kornuta, Timothy Kassis, Matt Nipper, and Mike Weiler) who have helped me to learn how to learn, a skill that will undoubtedly transcend my graduate school experience. I really enjoyed working in the lab with them, and my other lab mates, each day. I must also thank Dr. Tony Schmitz and Dr. Scott Banks, professors of mine at the University of Florida, who played instrumental roles in motivating me to pursue a graduate education at Georgia Tech.

I would like to thank my father (Rick), mother (Debbie), and sister (Kathryn) for the inspiring example that each has set for me, and the encouragement, wisdom, and love they have given me throughout my life. They have always allowed me to dream big and to chase my dreams. I am blessed beyond measure to call them my family. I would not be where I am today without my beautiful wife-to-be, Christin Nicole, who has been a loyal and patient supporter and helper to me throughout the past 6 years as I pursued my education in engineering. I look forward to many more years of learning with her and from her. All of my life and work are fundamentally indebted to the Savior of my soul, Jesus Christ, who has redeemed and freed me to experience life to the fullest.

TABLE OF CONTENTS

	Page
ACKNOWLEDGEMENTS	iv
LIST OF TABLES	vii
LIST OF FIGURES	viii
LIST OF ABBREVIATIONS	x
SUMMARY	xi
CHAPTER	
1 INTRODUCTION	1
Overview of the Lymphatic System	1
High-level Description and Function of the Lymphatic System	1
History of Discovery	2
Large Scale Anatomy	2
Small Scale Anatomy and Vessel Architecture	3
Lymphatic Physiology in Health	4
Lymphatics and Nitric Oxide	5
Results of Failed Lymphatic Physiology	6
Need for Diagnostics	6
Lymphatic Pumping Pressure	7
Description of Forces on the Vessel Walls	7
Methods of Blood Pressure Measurements	8
Overview of Lymphatic Imaging	10
Necessity and Advancement of Lymphatic Imaging	10
Injection Techniques	11

Imaging Techniques 12

NIR Imaging of the Lymphatics 15

Purpose for Using NIR Imaging 15

Previous Utilization of NIR Imaging with ICG Dye 16

2 "MINIMALLY INVASIVE ASSESSMENT OF LYMPHATIC PUMPING PRESSURE USING FUNCTIONAL NIR IMAGING" By: Akin, R., Weiler, M., Kassis, T., Dixon, J.B. 18

Introduction to Paper 18

Materials and Methods 22

System Design 22

In Vivo Imaging 24

Collection of Data 25

Data Analysis 29

Results 31

Discussion 33

3 CONCLUSION AND FUTURE WORK 40

REFERENCES 42

APPENDIX A: Log of Rats Used Throughout the Study 51

APPENDIX B: Intensity Plots for Rats included in Chapter 2 53

APPENDIX C: Labview Visual Instruments (Vis) and Code 61

APPENDIX D: Log of Anesthesia Administered to Rats 81

APPENDIX E: Log of Blood Pressure Measurement 83

APPENDIX F: Rat Log Used for Data Analysis 85

APPENDIX G: Results Data 88

APPENDIX H: Data Analysis Code – Courtesy of Dr. J. Brandon Dixon 90

LIST OF TABLES

	Page
Table A.1: Log of Rats Used Throughout the Study	52
Table D.1: Log of Anesthesia Administered to Rats	82
Table E.1: Log of Blood Pressure Measurements	84
Table F.1: Log of Rat Data Used for Analysis	86
Table F.1 (Continued): Log of Rat Data Used for Analysis	87
Table G.1 Results Data	89

LIST OF FIGURES

	Page
Figure 2.1: Pressure Cuff System Schematic	24
Figure 2.2: NIR Lymphatic Imaging System Schematic	25
Figure 2.3: Standard Pressure Curve	28
Figure 2.4: Data Analysis Plots	31
Figure 2.5: Results Plot	33
Figure B.1 Pressure Cuff Program GUI	54
Figure B.2 Rat 1	55
Figure B.3 Rat 2	55
Figure B.4 Rat 3	56
Figure B.5 Rat 4	56
Figure B.6 Rat 5	57
Figure B.7 Rat 6	57
Figure B.8 Rat 7	58
Figure B.9 Rat 8	58
Figure B.10 Rat 9	59
Figure B.11 Rat 10	59
Figure B.12 Rat 11	60
Figure C.1 Sequence 0	62
Figure C.2 Sequence 1	63
Figure C.3 Voltage Acquisition and Conversion to Pressure	64
Figure C.4 Filter	64
Figure C.5 Manual/Automatic Control Selection	65

Figure C.6 Case 1.0 68
Figure C.7 Case 1.0 False 69
Figure C.8 Case 1.1 69
Figure C.9 Case 1.2 70
Figure C.10 Case 2 70
Figure C.11 Case 3.0 71
Figure C.12 Case 3.1 71
Figure C.13 Case 3.2 72
Figure C.14 Case 4 72
Figure C.15 Case 5.0 73
Figure C.16 Case 5.1 73
Figure C.17 Case 5.2 74
Figure C.18 Case 6.0 74
Figure C.19 Case 6.1 75
Figure C.20 Case 6.2 75
Figure C.21 Sequence 3 76
Figure C.22 Serial Command Tab of Front Panel 77
Figure C.23 Syringe Pump Formatting Serial Commands 77
Figure C.24 Numeric Input to Syringe Pump 78
Figure C.25 Text Input to Syringe Pump 78
Figure C.26 Operation Tab of Front Panel 79
Figure C.27 Operation Tab of Front Panel – Execution Panel 80

LIST OF ABBREVIATIONS

BCRL	Breast Cancer Related Lymphedema
CT	Computerized Tomography
GTNO	Glyceryl Trinitrate Nitric Oxide
GUI	Graphical User Interface
ICG	Indocyanine Green
LEC	Lymphatic Endothelial Cell
MIR	Magnetic Resonance Imaging
MPS	Mononuclear Phagocyte System
NIR	Near Infrared Imaging
NO	Nitric Oxide
PET	Positron Emission Tomography
SPECT	Single-Photon Emission Computerized Tomography
USPIO	Ultrasmall Superparamagnetic Iron Oxide

SUMMARY

Although the major functions of the lymphatic system are fairly well defined, its vasculature has yet to be well characterized in comparison to its blood vasculature counterpart. Recent advances in optical imaging techniques have allowed for more detailed and quantitative evaluations of lymph flow dynamics and mechanism. A rat tail is often used for investigations of lymph flow because of the simple geometry, superficial nature, and disease progression models of its collecting lymphatic vessels. In this study, a pressure cuff system was fabricated and coupled with an existing functional near infrared (NIR) imaging system to measure the overall pumping pressure of the lymphatic vessels of a rat tail. In addition to adapting the system for use on rodents, previous systems used for measuring lymphatic pumping pressure in humans were improved upon in several ways. The system defined here utilizes closed-loop feedback control of pressure application at smaller, more precise intervals. Using this device, a significant difference in lymphatic vessel pumping pressure was detected between a control case and a treatment case in which a vasoactive substance with a nitric oxide donor (GTNO ointment) was applied to the tail. Although it is known that nitric oxide plays a crucial physiologic role in propagation of flow through lymphatic vessels, this study has quantified its significant pharmacological reduction of pumping pressure for the first time.

CHAPTER 1

INTRODUCTION

This chapter provides background information that will contribute to a better understanding of the thought processes behind the content of the study presented in Chapter 2. Additionally, it attributes credit to many of the influential scientists and engineers in the fields of lymphatics and imaging, although it should also be acknowledged that many others were intimately involved in paving the path for the presented research.

Overview of the Lymphatic System

High-level Description and Function of the Lymphatic System

The lymphatic system consists of a network of vessels, nodes, and accessory organs[1-3] that play a vital role in the body's balance of interstitial fluid volume to maintain protein concentration and oncotic pressure gradients.[1,4,5] In health it operates as an open system that returns excess interstitial fluid and proteins to the blood stream via a lymphatic duct in the left subclavian vein.[1,6] Additionally the system is essential to a wide variety of physiologic and pathophysiologic processes including immune cell trafficking and regulation of immunity,[7-9] lipid transport,[1,10] progression of autoimmunity,[1,11] cancer metastasis,[1,11] and tissue inflammation.[1,12,13] Current research continues to propel scientists toward a greater understanding of a system that has taken many contributors to realize.

History of Discovery

Discovery of the lymphatic system has taken place over the course of many years, possibly even dating back to 460 B.C.[1,13] It is really not well known when or where the lymphatics were initially noticed. Some writings suggest that great philosopher and scientists such as Hippocrates and Aristotle may have identified lymphatic structures, but these suggestions are based on writings of others and are unclear[1,14]. Even though speculation surrounds the first true identification of the lymphatics, recognition of their overall function is typically attributed to William Hunter in 1746.[1,15-17] However, his writings were preceded in 1654 by Francis Glisson who described part of the function of the lymphatic system in his book *Anatomia hepatis.*[1,3,17,18] In 1784 a contemporary of Hunter's, William Cruikshank, published one of the first all-encompassing books on the lymphatics titled *The anatomy of the absorbing vessels of the human body.*[1,4,19,20] This book described the history of discovery, anatomy, and physiology of the lymphatic system[1,21,22]. Not long after Cruikshank's book was published, in 1787 Paolo Mascagni published an incredibly detailed, and still relevant, atlas of the anatomy of the lymphatics.[7,23]

Large Scale Anatomy

A network of converging vessels comprises a significant portion of the lymphatic system. These converging vessels begin as very tiny, blind-ended tubes that are lined by endothelial cells and permeate the intercellular spaces of all tissues, except the brain and eye.[1,24] These initial lymphatics are closely related to the capillaries and small vessels of the circulatory system in the organs of the abdomen and thorax. In the limbs they primarily infiltrate the skin and subpapillary dermal plexus. Within the interstitial spaces

these tubes merge to form small vessels that continue to unite in the tissues around the blood venules and arterioles.[1,25] As these small vessels are increasingly joined together, they form large collecting vessels. These vessels lie in the subcutaneous, perivascular, retromediastinal and retroperitoneal tissues.[1,26] They are segmented into individual pumping units, called lymphangions, by macroscopic bileaflet valves every 2-3 mm that ensure proper unidirectional flow.[1,13,27,28] The collecting vessels run through the limbs and abdomen, eventually making their way to the thoracic duct, which connects to the left subclavian vein. Inside the lymphatic vessels is a substance called lymph, which is an almost-clear liquid composed of water, protein molecules, urea, glucose, salts, and white blood cells.[13,28] It also carries a variety of fats and fat-soluble vitamins that come from the gut. Collections of lymphoid tissue, known as lymph nodes, are found along the lymph vessels.

Small Scale Anatomy and Vessel Architecture

A discontinuous barrier of endothelial cells and basement membrane form the initial lymphatics. This intermittent membrane contributes to the ease of entrance into the lymphatic lumen of molecules, fluid, viruses, and bacteria.[14,29-31] Some studies suggest that small, funnel-like valves are present between the endothelial cells that regulate the entrance of fluid into the lumen and prevent backflow.[8,15,17,32-34] Other studies suggest that the endothelial cells are connected via interdigitating junctions implying that all junctions may not function as valves in the same way.[8,17,18] The outer endothelial cell layer is connected to matrix fibers via collagen VII anchor filaments.[8,19,20] Although there is no smooth muscle surrounding the initial lymphatics, there do appear to be branching cells that may have contractile properties.[21,22,35] The collecting lymphatics into which the

initial lymphatics merge are surrounded by smooth muscle, which enables their contraction.[23,30] The lumen of these vessels is formed by a layer of lymphatic endothelial cells (LECs) and a basement membrane that is surrounded by smooth muscle tissue. This membrane does not permit the entrance of the substances that can enter the initial lymphatic vessels.

Lymphatic Physiology in Health

The lymphatic system executes several functions when operating in health. The three main functions are maintenance of fluid homeostasis, response of the immune system, and absorption and transport of lipids. Its primary role in maintaining interstitial fluid balance is the intake of the fluid and transport of it back to the heart. The discontinuous cell layers around the initial lymphatics allow fluid and other substances to enter the lumen. From there the fluid, now termed lymph, is transported to the collecting lymphatic vessels, which act as a conduit to convey it back to the thoracic duct where it enters the blood stream. The transport of fluid through the collecting lymphatics is not a passive process, like the initial entrance of the interstitial fluid into the lumen. Several mechanisms help transport lymph against gravity and pressure gradients since the lymphatic system does not have a pump like the heart of the blood circulatory system. A combination of them enables movement of fluid through the lymphatic system at pressures lower than those in the blood vasculature in humans.[24,36] When functioning properly, it is estimated that the lymphatic system of a human returns around 8 liters of interstitial fluid to the blood stream each day.[25,37] Some extrinsic factors inducing flow are lymph formation, pulsations in the circulatory system, respiration, and muscle pumps during musculoskeletal movement[26,38,39]. Flow of lymph through the vessels is internally

perpetuated by sequential contraction of lymphangions.[27,28] The specialized smooth muscle cells surrounding the lymphangions are responsible for the phasic and tonic contractions that generate and regulate intrinsic pumping.[28] The bileaflet valves along the way prevent retrograde flow.

Lymphatics and Nitric Oxide

Several vasoactive substances are involved in the contraction and expansion process of lymphatic vessels including nitric oxide (NO) and endothelin-1.[29-31] The literature has shown that application of NO leads to a reduction in lymphatic transport.[8,32-34] One study shows that nitric oxide plays a role in lymphatic endothelial cell contraction under physiological conditions and that under inflammatory conditions it may be involved in the attenuation of contraction.[8] This same study suggests that cancer and infection may modulate immune response via NO regulation of lymphatic endothelial cell contraction[8]. In health, microscopic lymphatic endothelial cells release NO during contraction that causes dilation downstream.[35] This seems to play a significant role in lymphangion contraction propagation. In a cannulated vessel, it has also been made evident that NO release is correlated to frequency of lymphatic vessel contractions.[30] Increased fluid flow has also been shown to cause an increase in NO production and release by LECs of canine thoracic ducts.[36] These aspects of NO interaction with the lymphatic system make it a good substance for a treatment case to compare with a control case when measuring aspects of lymphatic pump function. The effects of NO on lymphatic pumping pressure have not been elucidated until now. Discovery of its pharmacological effects on the lymphatic vasculature could be beneficial for figuring out contributing factors to lymphatic disease as well as for developing treatments.

Results of Failed Lymphatic Physiology

Lymphatic system dysfunction can be caused by various diseases or alterations and can lead to an assortment of disorders.[37] While some lymphatic diseases are inheritable, others are the result of secondary causes. On a whole, lymphatic disease is rather wide-spread, but not clinically well-characterized.[38,39] Secondary lymphatic disorders are typically the result of disruption of lymphatic circulation produced by trauma, neoplasia, infection, or iatrogenic causes.[38] Another cause may be impairment of contractility of lymphangions.[40] When lymphatic flow is insufficient for maintaining proper fluid balance, excess fluid builds up in the interstitium and causes swelling, generally referred to as lymphedema. It is estimated that more than 130 million people[41] live with this often debilitating condition. One type of disorder resulting from iatrogenic causes in human females is breast cancer related lymphedema (BCRL). Studies report that after simple mastectomy or wide local excision with axillary clearance surgery there is up to a 1 in 4 chance of the patient developing BCRL.[42] However, the recent advancement of sentinel lymph node biopsy seems to have drastically reduced the chances of women developing BCRL.[42] This condition results in life-altering swelling of one or both of the arms and often leads to psychological difficulties.[43] Obviously psychological problems are not the only symptoms. Physically, lymphedema can lead to severe and irreparable fibrosis of tissue, cellulitis, and increased chances of skin cancer.[38,42]

Need for Diagnostics

Much of the damage caused by lymphedema and other lymphatic disorders and diseases is irreversible once it is well established. Current techniques are capable of

preventing the perpetuation of symptoms, but little success has been made in terms of eradicating them. Early diagnosis and treatment of symptoms can help prevent further long-term damage and lead to more positive patient outcomes. However, current diagnostics are primarily qualitative are only useful after the damage has been done. The current gold standard is confirmation via lymphoscintigram, but this procedure is time-dependent and inaccurate.[44] Another invasive technique is lymphangiography, but it is painful among other issues.[44] Non-invasive measurements in limb volume change are conducted using an ordinary tape measure to detect difference between limbs.[42] Otherwise, pitting edema detected after pinching the skin between the thumb and finger for 60 seconds or depressing the skin and qualitatively evaluating its return to normal are the best available indictors of lymphedema.[42] New diagnostics are needed for non-invasively detecting the onset of lymphedema so that progression of the disorder may be prevented or minimized.

Lymphatic Pumping Pressure

Description of Forces on the Vessel Walls

Just like the walls of any conduit of fluid flow, the endothelial cells lining lymphatic vessels experience hoop stress and shear stress. These stresses are functions of many contributing factors. It is well known that the lymphatic system must move fluid against a pressure gradient that is generated by (often negative) interstitial fluid pressure, central venous pressure, and the gravitational factor of hydrostatic pressure.[6] Specialized initial lymphatic structure, intrinsic pumping by lymphangions, and retrograde flow-preventing valves help to accomplish flow in this environment. It has been shown that in rat mesenteric lymphatic vessels a passive increase of lymph does not have much of an

inotropic effect on contraction, if any at all.[45] Obviously flow cannot occur intrinsically without contraction of the smooth muscle cells surrounding the collecting vessels. As one lymphangion contracts, the next lymphangion in the sequence experiences hoop and shear stress on its walls due to the volume of lymph ejected into it. This hoop stress has been termed the "pumping pressure" of the lymphatic vessel.

Methods of Blood Pressure Measurement

In determining this lymphatic pumping pressure, it is useful to evaluate some of the methods for measuring blood pressure. Non-invasive blood pressure measurement techniques include auscultatory, oscillometric, palpation, and pulse wave velocity methods. Each one has advantages and disadvantages, but evaluation of each may provide insight into potential lymphatic pumping pressure measurement techniques.

The pressure exerted on the walls of blood vessels has traditionally been measured using auscultatory methods. Initially blood flow is occluded in the arteries of the systemic circulation using a pressure cuff. Then the pressure is released until the clinician hears a "whooshing" sound with a stethoscope indicative of turbulent flow through the vessels. The pressure at which this auditory transition occurs is the highest pressure of blood flow in that portion of systemic circulation, during heart contraction, and thus represents systolic blood pressure. The clinician notes the pressure reading on the sphygmomanometer (pressure gauge) attached to the pressure cuff, and subsequently continues to deflate the cuff. When the pressure drops to a point when a sound can no longer be heard, the pressure is again noted. This lower pressure reading is representative of diastolic blood arterial pumping pressure, between heart contractions. Although

reasonably accurate, this technique of blood pressure measurement involves skill that is often slightly subjective.

Oscillometric methods are more automated than auscultatory methods and do not require the same training or skill. An automated pressure cuff is inflated beyond systolic blood pressure, and then steadily reduced to a pressure below diastolic blood pressure. During this deflation period, a pressure transducer (sensor) in the cuff detects the oscillatory properties of the pressure exerted on it due to pulsatile flow through the partially restricted vessel. The systolic and diastolic pressures are elucidated from internal calculations by the device rather than simply measured as in the auscultatory method. While this method has its advantages, it is also essential to use a pressure cuff that is the right size, because differences in cuff size can lead to differences in calculated pressures.

The simplest method of figuring out blood pressure is based on manual detection of the palpations at various anatomical locations. The ability to detect pulses in blood flow at some locations and not others can give a good indication of blood pressure ranges. For example, in a human, if a pulse can be detected at the carotid and femoral artery locations but not the radial artery location, then it can be deduced that the systolic blood pressure is >40 mmHg, and likely closer to 65 mmHg.[46]

Another method that is being researched but not utilized clinically is based on the pulse wave velocity principle. This method indirectly determines a value for blood pressure based on the pressure pulse velocity that is detected, which is indicative of blood pressure. In a rat tail, the arterial blood flow velocity measured with a Doppler ultrasonic probe was around 20 cm/s,[47] while lymphatic flow velocity measured using NIR imaging was around 0.15 cm/s.[32] Because of the relatively low velocity of fluid flow through

lymphatic vessels, the pulse wave velocity method may not be useful for elucidating lymphatic pumping pressure.

While these methods have proved useful for measuring arterial blood pressure in humans, they may not all translate well to use on a rat's lymphatic vessels. Sounds produced by lymphatic pumping would likely be drowned out by pumping blood, rendering auscultatory methods useless. Incredible sensitivity would be needed to measure pressure with the oscillometric method or pulse wave velocity method. Detecting palpations may be possible, but not by feel. Perhaps a combination of these methods would work best. One in which the cuff was operated as in the oscillometric method, the pressure was determined as in the auscultatory method (although visually rather than acoustically), and the determination was as simple as the palpation method. If pressure were to be measured visually, an imaging system capable of such visualization would be necessary.

Overview of Lymphatic Imaging

Necessity and Advancement of Lymphatic Imaging

There are several effective methods for measuring function of the blood vasculature. Contraction of the heart, the central pumping unit of the cardiovascular system, allows for the acoustic determination of blood pumping pressure. The high volume of flow through the vessels contributes to flow rates that are much higher than those through the lymphatic vasculature. The lymphatic vessels are relatively small and a central pumping unit does not drive flow through them. Therefore, acoustic determination of flow through lymphatic vessels is not feasible using current technology. Barring some bizarre use of another sense, the only other possible sense for measuring lymphatic flow

would be vision. In 1927, Egas Moniz was the first to use radiological methods for opacifying arteries and veins during life for the purpose of visualization.[48] However, visualization of the relatively tiny lymphatic vessels was beyond the scope of his work. Since the 1750s physiologists had known that colored dyes could be injected into the interstitial space to show up the lymphatics of animals.[1] However, the dyes that were used quickly diffused out of the lymphatic system due to their constituent small molecules.[1] After Patent Blue Violet dye became available with larger molecular size, Stephen Hudack and Phillip McMaster bravely injected themselves intradermally and where able to see their dermal lymphatics and the rapid spread of the dye.[49] It is likely that the first lymphographs involving X-Ray imaging of a contrast agent in healthy mammalian were those of a dog by William Glenn in 1948.[50] John Kinmonth was the first to produce lymphgiographs of human lymphatics in 1952, is often considered the father of lymphatic imaging.[51] These landmarks in lymphatic imaging have largely been the result of advancements in contrast agents and imaging techniques. The following sections outline the injection and imaging possibilities currently available for visualizing the lymphatic system in living subjects.

Injection Techniques

Contrast agents are required for the current methods of lymphatic system imaging, some of which are only useful for imaging lymph nodes, and some of which also enable the visualization of lymphatic vessels. The type of injection used has an impact on the resulting imaging capabilities. The three main methods of contrast injection are 1) direct endolymphatic contrast injection, 2) indirect interstitial contrast injection, and 3) indirect intravascular contrast injection.[52] Direct endolymphatic contrast injection is perhaps the

most logical. An oil-based contrast agent is injected into the lumen of a distal lymphatic vessel, which transports the agent proximally as expected. Opacification of the vessels allows for their imaging one day later, and imaging of the lymph nodes two days later.[52] Indirect interstitial contrast injection takes advantage of the large fenestrations in the lymphatic endothelial cells of the lymphatic capillaries.[53] The agent is injected into the interstitium and taken up into the distal lymphatic vessels along with other interstitial fluid being returned to the blood stream via the lympathic system. In lymphangioscintigraphy (discussed further in the following section) the agent injected into the interstitium has radioactive qualities that allow the vessels to be imaged using specialized gamma cameras.[52] This method has largely replaced direct endolymphatic contrast injection because it is safe, repeatable, and simpler, yet also provides functional and structural detail of the lymphatics.[54] Indirect intravascular contrast agents derived from iron particles have a tendency to be captured by mononuclear phagocytic cells and delivered to organs that exhibit immune functions due to their inhabitation by the mononuclear phagocyte system (MPS).[55] It has been demonstrated that ultrasmall superparamagnetic iron oxide (USPIO) particles are small enough to be able to migrate across capillary walls and seem to be taken up easily by lymph nodes.[56] Therefore, a single injection of such particles may be useful for targeting the lymphatics for imaging. This technique is innately less predictable, implying more difficult targeting of specific lymphatic vessels.

Imaging Techniques

There are several traditional imaging techniques that can be used in combination with the aforementioned injection methods to acquire useful images of the lymphatic

system. Lymphography is useful for imaging the structures of various components of the lymphatic system (e.g. lymph nodes, lymph ducts, lymph capillaries, and lymphatic tissues) via X-Ray after the injection of a radioactive dye. In this procedure direct endolymphatic contrast injection is performed via a catheter inserted in a distal vessel, which has typically been made visible by a prior subcutaneous injection of a colored dye. The proximal lymphatic system structures are opacified for viewing on the resulting X-Ray film, termed the lymphogram. Lymphangiography is very similar but only allows visualization of the lymphatic vessels, rather than all of the other lymphatic system components that can be viewed through lymphography. Another imaging technique involves computerized tomography (CT) images compiled from a series of projections that are tomographically rendered to create 3D depictions of lymphatic vasculature.[57] While these techniques are excellent for identifying structures of the lymphatic system, when trying to quantify lymphatic function they lack the temporal resolution required for visualization of pumping and flow. Also, they are difficult to execute clinically because of difficulties with introducing sufficient amounts of contrast agent to produce high quality X-Ray images.[57]

One alternative to lymphography is nuclear imaging, a category in which several different methods may be utilized. The contrast agents used for nuclear imaging are radionuclides that decay to generate either gamma photons or annihilation photons.[57] Two-dimensional images based on the locations of the radionuclides may be produced through gamma scintigraphy. Three-dimensional images may be produced using single-photon emission computed tomography (SPECT) which uses a series of images captured by a gamma camera rotated around the subject during imaging. Positron emission

tomography (PET) relies on the coincident detection of annihilation photons and detects more photons than SPECT.[57] These types of nuclear imaging are much more sensitive than the X-Ray-based imaging techniques and thus they require smaller doses of radiopharmaceuticals for detection of the lymphatics.[57] Lymphoscintigraphy is the most common type of nuclear lymphatic imaging, and is useful for producing 2D visualizations of the lymphatic system.[57] However, scintigrams take 20 minutes to 2 hours to acquire due to slow gamma camera integration times, rendering this method ineffective at capturing the dynamics of flow through lymphatic vessels.[57]

Perhaps the most detrimental downside to nuclear imaging is that subjects are exposed to ionizing radiation. This can be avoided by using magnetic resonance imaging (MRI). This type of imaging plays off of the interactions of nuclei with an odd number of protons and/or neutrons with radiofrequency pulses and an external magnetic field to produce high resolution images.[57] Magnetic resonance imaging can be combined with intravenous or interstitial injection of a dye to image the lymphatic system. The greatest advantage of an MRI over other techniques is its spatial resolution, but the temporal resolution is far too low for real-time dynamic imaging required for quantifying lymphatic pump function.

Ultrasound imaging utilizes the variance in acoustic properties of different types of tissue by sending high frequency waves into the tissues and collecting the resulting echoes with a piezodetector on the surface of the skin. Lymphatic filariasis, the most common global lymphatic disease condition, and even live adult filarial worms have been imaged using ultrasonography, which can detect vessel dilation due to worm infestation.[58] While ultrasound has traditionally been used to image structure more than

function, it has recently been used for determining function in the lymphatics as well. Certain microbubble contrast agents seem to have an affinity for the lymphatic system and may be used for tracking flow in a process called lymphosonography.[59] Intravascular imaging advancements in this field may lead to more effective ways to image movement of fluid through the lymphatic system, but for now this is not the best way to image lymphatic function.

NIR Imaging of the Lymphatic System

Purpose for Using NIR Imaging

A sensitive camera can detect fluorescence emission from a fluorophore during *in vivo* fluorescence optical imaging. Fluorophores are simply fluorescent chemicals that emit light after they are excited by an excitation source. Their molecules emit light upon relaxation to their neutral state after they have been excited to a higher energy level due to absorption of a photon during excitation.[57] The wavelength of re-emission is longer than that of excitation so a filter-fitted camera can distinguish between the two. While fluorophores are typically non-active and non-targeting on their own, they may be bound to macromolecules to enable targeting of specific body systems or cell types. The dyes may be injected in any of the three previously described ways.[57] Used primarily for evaluating blood flow and clearance, the only near-infrared *in* vivo fluorophore that is approved for clinical use is Indocyanine Green (ICG).[60]

Contrary to fluorescence microscopy, which is confined to imaging cells on slides or in culture dishes, fluorescence imaging on the macro scale allows for real-time imaging of live, physiological systems in whole animals.[61] One issue with some types of fluorescence imaging is that after some tissues are excited with certain wavelengths of

light during laser penetration aimed at the fluorophore, they emit their own additional light, which is termed autofluorescence.[62] Because physiological tissues generate very little autofluorescence in the infrared spectrum of light, macromolecules that emit these wavelengths (700-1000 nm) are more efficient for visualizing target tissues *in vivo*, especially deep tissues.[60,62] This rules out quantum dots (QD's) as a fluorophore because they are excited with visible light and are therefore ineffective for deep tissue imaging.[57] In addition to keeping excitation and emission peaks at wavelengths above about 650 nm to prevent autofluorescence, it is also beneficial to keep them below about 950 nm to prevent disruptive light scattering and tissue heating.[60] As long as these precautions are obeyed, NIR imaging may provide a clinically relevant and relatively inexpensive way to image the lymphatic system.[57] Additionally, it is currently the only way to image propulsion of flow through collecting lymphatic vessels *in vivo.*[63] The ability to image propulsion of lymph through vessels in swine,[63] mice,[64] and humans[65] has been demonstrated. Therefore, it may be the ideal imaging method for visualization flow through lymphatic vessels during pressure measurement.

Previous Utilization of NIR Imaging with ICG Dye

In recent years NIR imaging has gained popularity as its effectiveness has been exhibited in various studies. In 2000 it was shown that NIR imaging techniques in conjunction with intravenous injection of ICG dye allowed for the monitoring of its pharmacokinetic delivery in tissue depths of up to 0.5-1 cm.[66] Discretized "packet" flow through the lymphatics was observed in an anesthetized swine after intradermal ICG injection.[63] Kitai et al. used subcutaneous injection of ICG with NIR imaging to detect subcutaneous lymphatic vessels and sentinel lymph nodes (SLN), which are those to

which tumors primarily drain.[67] Others have used this combination to detect dilation of lymphatic vessels in lymphadematous limbs as compared to healthy limbs in humans by mapping the lymphatic system.[68] The same group was also able to detect age and gender specific differences in human lymphatic vessel pumping pressure recently by using NIR imaging.[69] Indocyanine green has also been used with NIR imaging to quantify lymphatic function in breast cancer patients.[65] Although ICG cannot be conjugated with a targeting peptide, protein, polysaccharide, or other molecule, it can be non-covalently bound to albumin to form a lymphotropic agent.[57] After binding to albumin, the resulting molecule is too large to enter the blood vasculature, and it may only enter the lymphatic vasculature due to the larger fenestrations in the LEC membrane. The combination of NIR imaging and ICG dye has proven useful for evaluating lymphatic pump function.[32,70]

CHAPTER 2

"MINIMALLY INVASIVE ASSESSMENT OF LYMPHATIC PUMPING PRESSURE USING FUNCTIONAL NIR IMAGING"

BY: AKIN, R., WEILER, M., KASSIS, T., DIXON, J. B.

This chapter includes a journal article submitted for publication to the peer-reviewed American Heart Association – Circulation Research journal that has been extended to provide more detailed content for the reader than would be necessary for a published article.

Introduction to Paper

The lymphatic system consists of a network of vessels, nodes, and accessory organs[2] that play a vital role in the body's balance of interstitial fluid volume to maintain protein concentration and oncotic pressure gradients.[5] In health it operates as an open system that returns excess interstitial fluid and proteins to the blood stream via a lymphatic duct in the left subclavian vein.[6] Additionally, the system is essential to a wide variety of physiologic and pathophysiologic processes including immune cell trafficking and regulation of immunity,[8,9] lipid transport,[10] progression of autoimmunity,[11] cancer metastasis[11] and tissue inflammation.[2,12] After uptake by the initial lymphatics, flow of lymph through the vessels is internally perpetuated by contraction of individual pumping units known as lymphangions.[5,27,28] Other mechanisms inducing flow include extrinsic factors such as lymph formation, pulsations in the circulatory system, respiration, and muscle pumps during musculoskeletal movement.[6,26] A combination of these

mechanisms moves fluid through the lymphatic system at pressures lower than those in the blood vasculature in humans.[8,9,71]

While it is likely that the molecular and biophysical mechanisms that control lymphatic pumping are quite complex, nitric oxide has recently emerged as one of the key regulators in this process.[72] For example, it is involved in the flow-induced inhibition of lymphatic vessel pumping in cannulated mesentery lymphatics.[10,73] Also, peaks of nitric oxide release have been observed *in vivo* in temporal and anatomical regions of higher shear stress in the lymph vessel.[30,35] Nitric oxide has also been shown to be a regulator of lymphatic function and/or growth in several pathophysiologic or inflammatory conditions.[8,74-77] Lastly, the application of a NO-containing ointment dermally reduces lymphatic transport through the lymphatic vessels.[11,32] The ability to quantify the role of nitric oxide in the physiologic responses of lymphatic function in animal models of lymphatic disease is crucial for understanding and developing efficacious therapies for treating these conditions.

More than 130 million individuals worldwide suffer from lymphedema, a chronic disease that presents with the accumulation of fluid, proteins, and adipocytes in the interstitium, resulting in a drastic enlargement of the affected limb.[11,41] Currently there is no cure for lymphedema and our understanding of the factors that contribute to disease progression are minimal at best. While a few known mechanisms have been associated with lymphedema development, such as valve malfunction (through abnormal development or deterioration) and faulty lymphatic vessel formation (lymphangiogenesis),[40] it is unknown how the primary driver of lymphatic flow – the intrinsic pumping capability of lymphangions – is involved in the disease. Post-hoc

analysis of lymphatic vessels in humans and various animal models affected by lymphatic dysfunction have suggested alterations in lymphatic vessel smooth muscle coverage.[78,79] However, it is unclear how these changes directly impact lymphatic pumping and the role that this plays in driving disease progression. It is also possible that early changes in lymphatic pumping capacity could be a sign of disease risk, informing patients of the state of their lymphatic health. While pressure has been measured in exteriorized rat vessels,[80] the ability to obtain a minimally invasive pressure measurement of the lymphatic system *in vivo* is essential for studies with animal models investigating the longitudinal functional response of lymphatics to variations in pump demand and the role of pump failure in lymphatic disease. The techniques reported here were applied to the rodent tail model. This was chosen due to its ideal symmetry and the unidirectional nature of lymphatic flow in this limb. Additionally, the rodent tail model is one of the most widely used models in lymphatic research and has provided insight into basic lymphatic physiology and lymph flow,[32,81] lymphangiogenesis[82-85] and lymphedema pathology.[86-88]

One of the current limitations in animal models in lymphatic research is the paucity of applicable *in vivo* imaging techniques.[89] While numerous techniques have been used to visualize lymphatic drainage including lymphoscintigraphy, MRI, and PET, they have yet to be utilized routinely due to their prohibitive cost and/or lack of appropriate sensitivity.[57,63,90-92] The advancement of Near Infrared (NIR) imaging has made it possible to visualize and measure quantitative metrics of lymphatic function.[89,93,94] Minimal autofluorescence and reduced absorption/scattering in biological tissues at the depths of superficial lymphatic vessels make near-infrared wavelengths

ideal for this application.[32] An FDA-approved fluorophore, indocyanine green (ICG), can be excited by a laser diode after uptake into the lymphatics via intradermal injection to emit infrared light, which is then captured by a CCD camera fitted with an appropriate filter.[68] Various quantitative metrics have been used to characterize lymphatic pump function *in vivo* by employing this technique including flow velocity, packet frequency, and transport time.[32,63,89] While these techniques provide information regarding the temporal dynamics of lymph transport, they cannot measure the pumping pressure in the vessels.

Two important developments have been made recently in this regard. By utilizing an occlusion cuff to stop lymphatic flow in humans, and then measuring the pressure at which flow is restored by visualizing lymphatic transport with either lymphoscintigraphy[95] or NIR imaging,[70] Mortimer et al. and Unno et al. were able to report significant differences in pumping pressure between normal patients and those with advanced lymphatic disease symptoms. However, the measurements themselves were subject to a high degree of variability across each patient group, as well as a high degree of variability when comparing one technique to the other.[69,70] This could be due in part to the limited pressure resolution (10 mm Hg) of the manual and open-loop approach used for the application of pressure. Given these limitations, along with the desire to measure the effects of nitric oxide on lymphatic pumping pressure, this general approach was built upon to develop a novel, *in vivo*, minimally invasive animal imaging system to measure lymphatic pumping pressure.

Methods and Materials

System Design

A closed-loop pressure cuff system (Figure 1) was devised that made use of a pre-existing pressure cuff (Kent Scientific, Torrington, CT), which was manufactured with the intended purpose of blood occlusion. It is typically an integral part of a rat blood pressure measurement system where it is inflated to occlude blood flow while volumetric change of the tail is measured with a separate component of the system. Kent Scientific offers multiple sizes of the cuff, which could be used to perform experiments on various sizes and species of rodent tails. The rigid cylindrical structure of the cuff is made out of plastic, and the deformable bladder is made out of a thin-walled tube of elastic polymer. The tube is threaded through the rigid plastic cylinder, and the ends of the elastic piece are stretch around the outside of it. Two O-rings are used to attach the elastic tube to the plastic piece. After multiple experiments the elastic piece can be changed out with one of the replacements that comes with the occlusion cuff when it is ordered. Each complete occlusion cuff kit includes the plastic cylindrical piece, multiple pieces of elastic thin-walled tubing, replacement O-rings, and some tubing attached to the plastic cylinder ending in a luer-lock fitting to attach it to an inflation device.

The pressure cuff was attached to a 3 mL BD luer-lock syringe via plastic tubing (1/16” ID, 1/8” OD) and to a pressure transducer (Honeywell Sensing and Control, Morristown, NJ) via a plastic barbed T-fitting and additional plastic tubing (1/8” ID, 1/4" OD). A 3 mL syringe was chosen strategically because of its diameter. An equivalent movement of the plunger of a larger diameter syringe would translate into a much larger change in pressure in the system. However, if the diameter were much smaller the

response time of the system would be longer due to limitations of actuator speed. Also, the 3 mL syringe allowed for enough volume change to cause the necessary 80 mmHg change in pressure. A 0~1 bar (0~750.061683 mmHg) ±0.25% gauge pressure transducer providing an analog output (Digi-Key Part Number 480-3299-ND) was chosen to measure the pressure in the system.

The pressure transducer was attached to a data acquisition (DAQ) device (National Instruments (NI), Austin, TX) to feed it 5V of supply and to acquire voltage values proportional to pressure sensation. The NI DAQ USB6009 was already available in the lab and easy to use. It also had a high enough sampling rate to acquire the desired signals. Three electrical wires were fed into the DAQ: one into the Analog Output 0 (AO0) port, one into the ground port on the same (Analog) side, and one into the 5V supply port. The other ends of these three wires were all connected to the pressure transducer. The DAQ device was connected to a computer (Windows 7 32-bit) via a USB cable. The voltage fed into the DAQ via the AO0 port was then accessed by a customized LabView virtual instrument (VI) (NI, LabView 2012 32-bit) and used to make decisions about the serial command output to the syringe pump (Harvard Apparatus PHD 2000 Infusion/Withdraw 70-2001). The serial command was transmitted from the computer to the syringe pump via a USB cable connected to an RS-232 cable. Cable adapters were necessary for transmission of data. The linear pump was then used to modulate displacement of the syringe plunger, thereby altering the volume and pressure of air inside the closed-tube system. To ensure a fast response for large changes in pressure and good steady state tracking the syringe pump was commanded to operate at a slower speed when the experimental pressure was within 7 mmHg of the desired pressure.

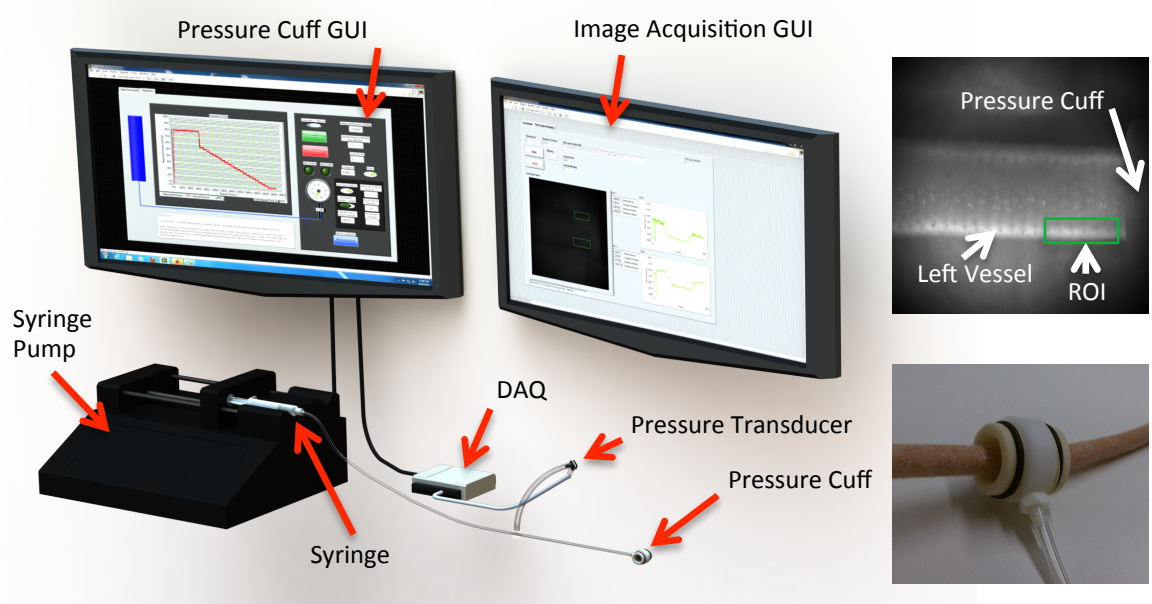

Figure 1 Pressure Cuff System Schematic (Left) An automated, integrated, feedback-controlled, lymphatic pumping pressure and imaging system with user interfaces serves as a powerful toolset for lymphatic physiology. A CAD model of the pressure cuff system including labeled depictions of its various components is shown. (Right top) A sample image of a rat tail during an experiment with an example ROI identified. The pressure cuff can be seen at the right of the image. While two lymphatic vessels can be seen along the sides of the tail, the excitation source was focused on the lower vessel, which was used for quantification. (Right bottom) Image of the pressure cuff placed on a rat tail.

In Vivo Imaging

The NIR imaging system was set-up as described previously by Weiler et al. (Figure 2).[32] A diode driver and temperature control box powered a 1 W 808 nm laser diode (Thorlabs, Newton, NJ), which provided excitation light. To disperse the laser over a larger area of approximately 75 cm^2 with less than 1.9 mW/cm^2, a 20 degree beam diffuser (Thorlabs, Newton, NJ) was fixed in front of the diode. An Infinity K2/SC video microscope lens (Edmund Optics, Barrington, NJ) and a bandpass filter (CW: 840 nm, FWHM: 15 nm, Omega Optical, Brattleboro, VT) were attached to a PIXIS 1024B back-

illuminated CCD camera (Princeton Instruments, Trenton, NJ) to capture fluorescence emission centered at 840 nm. These wavelengths were chosen based on previous work that showed that ICG undergoes a spectral shift when it binds to albumin.[32] The camera was connected to the same computer as used for the pressure cuff system, where the images were acquired by an additional custom LabView VI displayed on a second monitor.

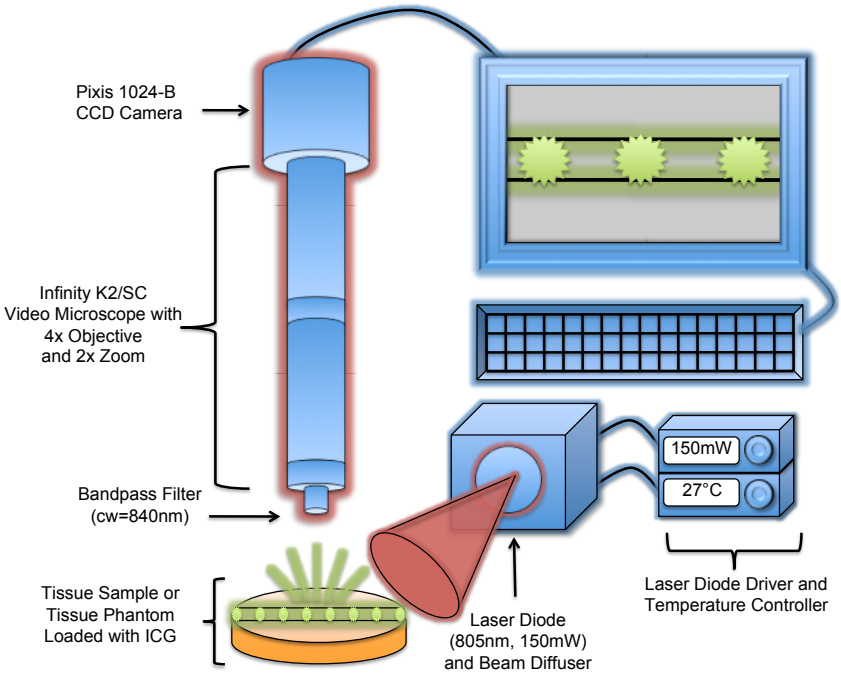

Figure 2 NIR Lymphatic Imaging System Schematic. Excitation light is provided by 1 W 808 nm laser diode powered by accompanying diode driver and temperature control boxes.[32]

Collection of Data

A standardized procedure was carried out on eleven, nine week old, albino Sprague Dawley (Charles River, Wilmington, MA) rats. Briefly, 30 uL of ICG/albumin solution (150 μg/mL ICG (Acros Organics, NJ) and 60 g/mL bovine albumin (MP

Biomedicals, Auckland, New Zealand) dissolved in deionized water was injected intradermally at the tip of the tail as described previously.[32] The injection site was typically within 1 cm of the tip of the tail and the needle was positioned to puncture the skin at about a 30 degree angle before rotating it to a position more parallel to the tail for further penetration. The needles used for ICG injection were 29 gauge with a 3/10 cc syringe. Six rats received a topical application of glyceryl trinitrate ointment (GTNO) (0.2% wt⁄wt, Rectogesic, Care Pharmaceuticals, commercially available) applied on the exterior of the tail, while the remaining five control rats received no GTNO ointment. The ointment was uniformly distributed on the epidermis of the tail manually. Some variation in application of the ointment was certainly likely. It has been shown that the NO donor group contained in this ointment slows lymphatic transport time.[32,34] In order to minimize light scattering, a depilatory lotion was used to remove hair in the region of interest on the tail one day prior to experimentation. To keep the rats stationary during hair removal they were anesthetized using Isoflorane. During the pressure determination experiments rats were anesthetized with an intramuscular injection of Diazepam (2.5 mg⁄kg) followed by a cocktail of Fentanyl (0.12 mg⁄kg) and Droperidol (6 mg⁄kg). Weight-dependent doses were administered to each rat. After waiting for approximately 10 minutes for the anesthetics to take effect the rat was positioned under the camera. The pressure cuff was calibrated by detaching and reattaching the tubing connected to the syringe and ensuring that the steady state pressure was zero. During an initial calibration of the pressure transducer, voltage values were recorded while the system was open, then averaged, and a calibration constant was entered to account for the discrepancy from zero. Then the cuff was fitted onto the tail at a position where its inner diameter was

uniformly touching the tail without applying any pressure, as verified by pressure transducer readings. This placement was typically about 11 cm from the tip of the tail, placing it about 4.5 cm from the base of the tail. Also, the cuff was positioned in the same rotational orientation for each rat to compensate for any non-uniformities in pressure application by the elastic bladder during inflation. The rat was positioned so that the field of view was proximal to the cuff, including only the edge of the cuff.

The image acquisition began just prior to intradermal injection of 30 μL ICG dye. Once steady state fluorescent flow was established, more than 3 minutes after injection, a predetermined sequence of pressure cuff applications was administered to the tail. Specifically, the pressure was increased to 80 mmHg over a period of about 65 seconds and held at this value for 10 minutes. This pressure was chosen for lymph flow occlusion because it was more than sufficient in previous trials. Also, 80 mmHg is close to the diastolic blood pressure of a rat, and well below the average BP, so blood was not occluded during the experiment.[96] After remaining at 80 mmHg for 10 minutes, the pressure was decreased to 55 mmHg over a period of about 25 seconds. The pressure was then decreased at increments of 2.5 mmHg after remaining at each pressure value for 60 seconds, until the pressure value was zero, where it remained for 3 minutes before terminating the program. The system took less than 15 seconds to respond to each decrement in pressure. This standardized pressure curve, shown in Figure 3, was used for all 11 experiments.

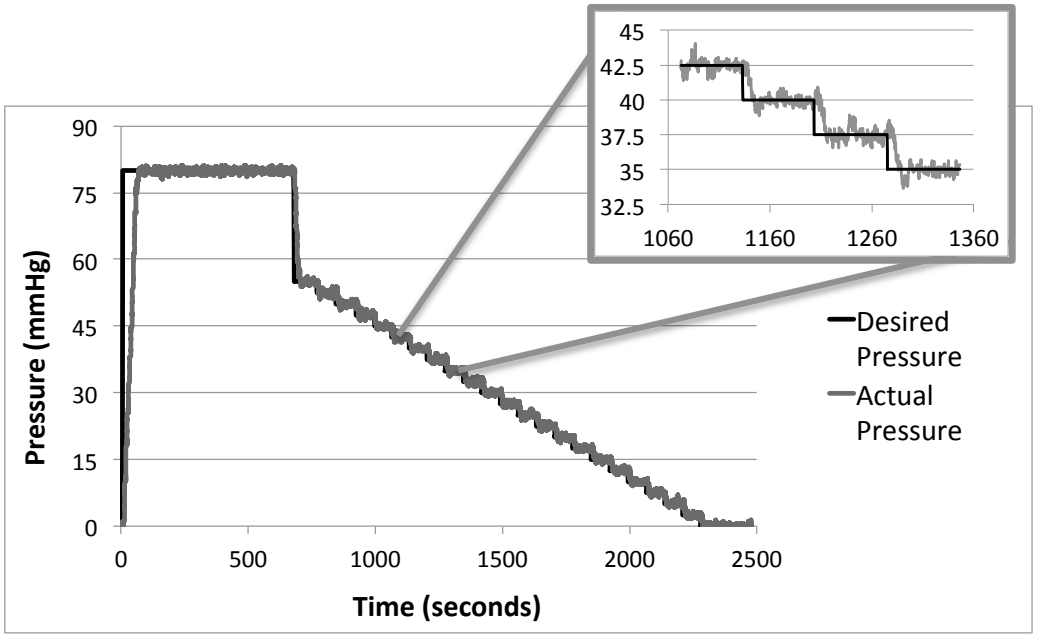

Figure 3 Standard Pressure Curve. Feedback-controlled pressure curves are applied to the tail with sufficient precision and speed. A pressure curve representative of that used to apply pressure during each experimental trial is shown. The exploded image shows the close tracking of the filtered actual pressure to the desired pressure. Root mean squared error for the entire pressure curve (disregarding the initial ramp up to 80 mmHg) for this curve is 1.821 mmHg. Steady state root mean squared error during the 10 minutes at 80 mmHg is 0.477 mmHg. The actual pressure data was filtered throughout the experiment using a 5 data point mean filter. The reported mean squared errors are based on this filtered data.

Images of the tail were captured by the NIR imaging system throughout the experiment at a frame rate of approximately 1 fps with a camera exposure time of 0.05 s. After the first frame was captured, the system paused to allow the user to select 2 regions of interest (ROIs) that were just proximal to the pressure cuff, and surrounding the fluorescent vessels (Figure 1). The mean intensity in the ROIs was calculated real-time and displayed on two plots throughout the procedure. The ROI selected for use in the data analysis was always the one positioned over the left vessel of the tail. This was done both

for the sake of consistency and to optimize the optics for achieving the best signal on a single vessel. To optimize the optics the laser diode was positioned so that it produced the maximum fluorescence of the left vessel. Also, camera shutter malfunctions throughout many of the trials produces detrimental noise in the intensity value collection associated with the right vessel, therefore rendering it useless. Also, it appeared that the pressure cuff did not inflate uniformly around its circumference so, while consistency was seen in the left vessel, there were often differences in flow restoration between the two vessels. These differences could have been due to a dominant vessel. However, because the differences were consistent throughout several trials, the more likely cause was non-uniform inflation of the cuff. Therefore, the cuff was always oriented on the tails the same, and only data from the left vessel, which remained more consistent throughout previous trials, was used in the analysis.

Data Analysis

Two primary measurements were taken from each intensity plot and pressure curve combination (Figure 4) using customized data analysis algorithms written in Matlab. The first was "Pumping Pressure" (P_{pump}), which was determined to be the pressure corresponding a particular point on each intensity plot. This metric of "Pumping Pressure" is meant to be an overall assessment of lymphatic vessel contraction ability produced by intrinsic and extrinsic factors rather than a determination of luminal pressure, which would currently require a more invasive and physiologically altering procedure. The point chosen was where the intensity value rose to that of the minimum value during clearance of the vessel plus one half (50%) of the difference between that value and the maximum subsequent value. This correlates to the pressure when intensity

values reached half of their maximum values relative to their minimum values for each trial. To make sure the relatively arbitrary choice of 50% return was not a significant flaw in the data analysis process, pressure values were also extracted for the points on each intensity plot when flow had been restored by 10% and 20%. Also, three lab members were each instructed to choose a point on each intensity plot that they thought was most indicative of flow restoration in a blind study. The pressure values corresponding to each of their responses were averaged to provide a fourth method of pressure determination for each trial.

The second parameter that was determined was the pressure of "Packet Restoration". NIR imaging of lymphatic uptake produces discrete "packets" of fluorescence travelling through the vessel that are a result of the intrinsic contractility of the lymphatic vessels working in coordination with lymphatic valves. The frequency of these packets has previously been reported as a measurement of lymphatic function.[32] To determine the pressure at which packet flow was restored in the lymphatic vessel, an FFT was used to calculate the power of the signal in the frequency range of 0.06 – 2 Hz during both flow blockage (at 80 mm Hg) and after complete flow restoration (i.e. at 0 mm Hg). The pressure at which the frequency of packets (as determined by the same FFT algorithm) was restored to 50% of their maximum value was recorded as the Packet Restoration Pressure. The Packet Restoration metric was meant to identify the pressure when packets were evident that rivaled those seen during uninhibited flow. For two of the rats, one from each treatment group, packet flow was never detectable, neither before nor after inflation of the cuff. Therefore, no Packet Restoration value was determined for these rats.

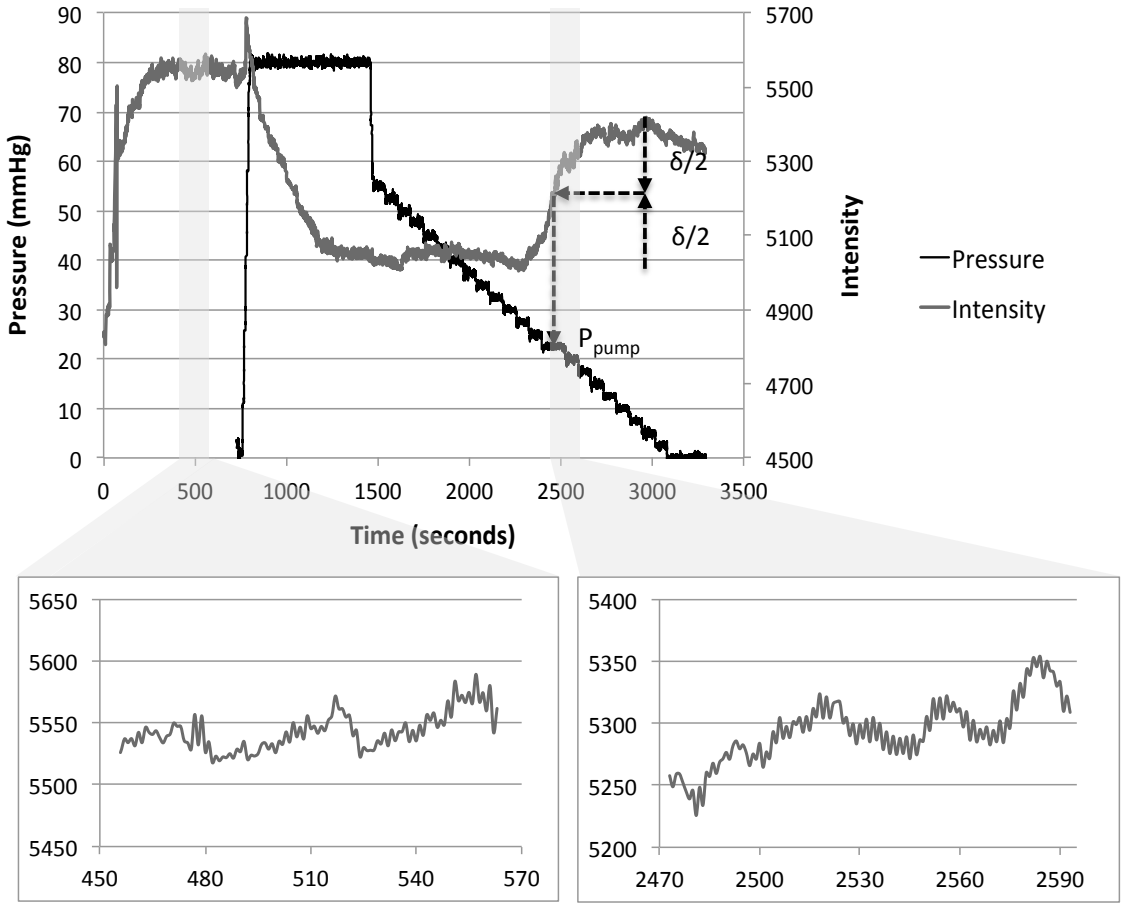

Figure 4 Data Analysis Plots. (Top) Multiple metrics of lymphatic pumping pressure and pump performance can be extracted from vessel fluorescent intensity plots. Overlaid pressure and intensity plots demonstrate the calculation of pumping pressure (P_{pump}). The time corresponding to the intensity value that was half way between the minimum value during no flow and the maximum value after flow restoration (representing the 50% flow restoration case) was determined. Then the pressure corresponding to that time was established to be the pumping pressure. This was repeated for 10% and 20% flow restoration. (Bottom left) A highlighted section of the intensity plot representing packet flow before inflation of the cuff during uninterrupted flow. (Bottom right) A highlighted section of the intensity plot representing packet flow after flow restoration.

Results

Aided by the real-time feedback of the pressure transducer, the closed-loop system allowed for steady-state tracking of the desired pressure with an overall root mean squared (RMS) steady state error of 0.48 mmHg excluding the initial ramp-up to

80mmHg (Figure 3). The data was filtered through a five data point mean filter during the procedure, prior to analysis. Fluctuations at steady state were mostly due to noise in the pressure transducer measurements. The rise and fall times were fast enough for accomplishing the purposes of this experiment while avoiding significant undesirable overshoot. Overdamping of the system was acceptable since the duration of the experiment was not a primary concern.

Nitric oxide, via application of the GTNO ointment, significantly reduced lymphatic pumping pressure *in* vivo from 36 mmHg to 18 mmHg (Figure 5) as determined by the functional NIR lymphatic pumping pressure imaging system ($p<0.01$). These values were determined by the use of the 50% flow restoration metric during data analysis. The average pressure values as determined by the points at which flow had been restored by 20% were 45 mmHg for the control cases and 26 mmHg for the GTNO treatment cases ($p<0.05$). The third method of flow restoration determination was that of 10% restoration of flow. This method did not show a significant difference ($p>0.05$) between pumping pressures associated with the control and treatment cases respectively. Nitric oxide did however significantly reduce lymphatic pumping pressure from 36 mmHg to 26 mmHg as determined the blind study with three individual lab members evaluating the points of flow restoration on the intensity plots ($p<0.01$). Additionally, GTNO also significantly reduced the average pressure of packet restoration from 35 mmHg to 15 mmHg ($p<0.05$). There was no statistical difference between the two metrics of lymphatic pumping pressure (P_{pump} and Packet Resume) that were calculated for this study ($p=0.6$). Blood pressure in the tail, with a subset of rats ($n = 4$), was measured before and 20 minutes after GTNO application to determine the extent to which

the dermal NO application might have altered it. No statistical differences were observed in either systolic or diastolic blood pressure (Appendix G).

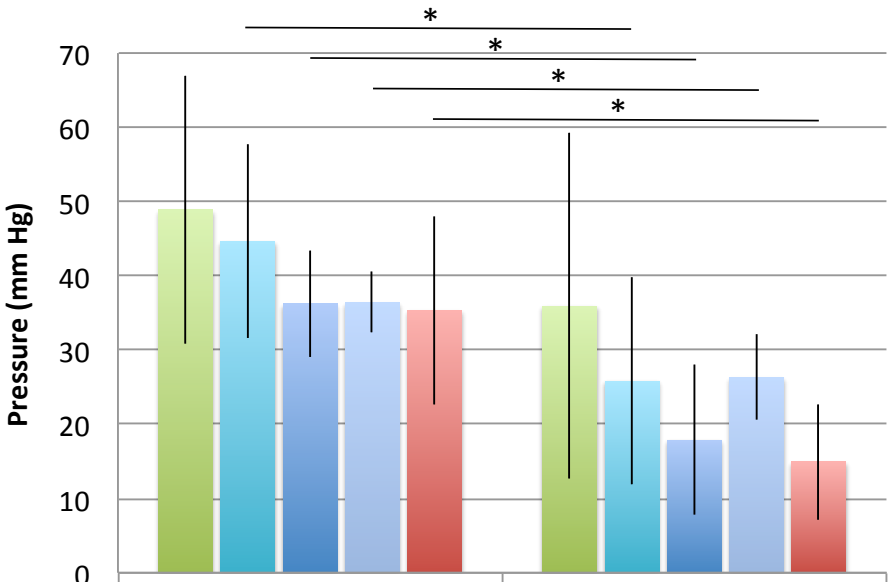

	Control	Treatment
Ppump - 10% Return	49	36
Ppump - 20% Return	45	26
Ppump - 50% Return	36	18
Ppump - Lab Member Avg	36	26
Packet Restoration	35	15

Figure 5 Results Plot. Nitric oxide significantly reduces lymphatic pumping pressure in 3 of the 4 methods of pressure determination through data analysis. The pumping pressure as determined using the 20% ($p<0.05$), 50% ($p<0.01$), and Lab Member Avg ($p<0.01$) metrics was significantly reduced as a result of a topical application of the nitric oxide releasing cream GTNO. The same was true for the pressure at which packet flow was restored ($p<0.05$).

Discussion

The disparity of research that exists between the lymphatic circulation and its vascular counterpart can largely be attributed to a lack of available tools for studying lymphatic physiology. The ability to monitor pressure and hemodynamics in the blood

circulation has been crucial for both assessing vascular health in a clinical setting and for probing the molecular mechanisms that regulate vascular biology in a laboratory setting. Development of technologies that enable similar measurements in the lymphatic vasculature in a non-invasive, or minimally invasive fashion such as that reported here, have the potential to have a substantial impact on the future of lymphatic research. The utility of the described lymphatic pumping pressure system has been demonstrated by reporting the effects of nitric oxide on lymphatic pumping pressure *in vivo* and with minimal invasiveness for the first time.

The findings are consistent with previous works, which have demonstrated a reduction of lymphatic transport with the application of NO.[8,32-34] In fact, it is becoming apparent that NO is a primary mechanism utilized by lymphatics to regulate flow. Specifically immune-cell released NO has been proposed as a mechanism for manipulating lymphatic flow as part of a local immunomodulatory response to inflammation.[8] Also transient changes in wall shear stress have been shown to result in NO release as a means of promoting vasodilation and reducing vascular resistance to flow.[30,33,35] While the above-mentioned studies all involved highly invasive procedures or experiments on surgically isolated lymphatic vessels, two recent reports non-invasively demonstrated a reduction in lymph transport due to NO.[32,34] However, the system developed here provides the first direct evidence *in vivo* that this reduction in lymphatic function results in a loss in lymphatic pumping pressure. More importantly, since the technique is minimally invasive it allows for one to take multiple measurements of lymphatic pumping pressure during the course of longitudinal studies in which it is hypothesized that there is a functional decline in lymphatic pumping capacity during

disease progression. In addition to measuring differences in pressure upon perturbation with NO, the data suggests that nominal lymphatic pumping pressure in rats is about the same as that in humans, just as blood pressure is similar in both species,[97,98] thus further validating rodent models as beneficial systems for studying functional lymphatic physiology.

While the general approach of using an occlusion cuff to stop lymphatic flow as a means of determining the pumping pressure was pioneered previously in humans,[70,95] there are some substantial differences in the presented approach that improve the accuracy of the technique as a laboratory research tool. First, by utilizing a computer-controlled, closed-loop control system to generate the desired pressure curves, greater precision and sensitivity were achieved than with previous manually controlled, open-loop feed-forward systems.[70,95] Additionally, by utilizing a highly sensitive optical approach that was previously optimized for lymphatic imaging[32] improved spatial and temporal resolution were achieved over lymphoscintigraphy.[95] Also, only $1/10^{th}$ of the volume (30 uL vs. 300 uL) of contrast agent injected into the interstitium was required compared to other reported NIR pumping pressure systems.[70] This is important, as large volume injections will introduce an abnormal interstitial fluid pressure downstream of the lymphatic vessel, possibly masking the true pumping pressure of the lymphatic vasculature. Additionally, the system we have developed allows for measurement of other functionality parameters of pumping including transport time, packet frequency, and packet velocity during the same experiment as described previously.[32]

Throughout the experimental process, consistency was maintained for as many variables as possible. However, there are some limitations of the technique that are worth

mentioning. First, the extent to which different tissue compliances, particularly in the axial direction, could have altered the actual pressure transmitted from the cuff to the vessel have not been considered. While this is not problematic for the current study since it is unlikely that NO would alter tissue compliance, further validation needs to be done when the approach is utilized to compare pumping pressures at sites with known compliance differences. Second, the physiological effects of anesthesia on the lymphatic pumping pressure are unknown. This could be problematic in studies where it is suspected that the anesthesia itself might mask hypothesized losses in lymphatic pumping pressure. Nitric oxide is also a known vasodilator of the vasculature, lowering blood pressure,[99] thus any effects of GTNO application on blood pressure would influence the perceived lymphatic pumping pressure. This does not appear to be the case as no differences in blood pressure were detected with the delivery method of NO. Interestingly, NO has been shown to increase capillary hydraulic conductivity,[100] which would enhance lymph formation, increase interstitial fluid pressure, and promote lymphatic flow. However, GTNO has the opposite effect, drastically reducing every metric of lymphatic function including pumping pressure,[32] suggesting that the local effects are primarily affecting lymphatic function. Perhaps the most uncertainty arises from the lack of knowledge about how interstitial fluid pressure is dispersed throughout the tail and how slight variations from one injection to another would affect lymphatic pumping pressure. While as much standardization as possible was attempted during each injection, the application of microneedles to deliver the contrast agent at defined depths with very precise volumes is a future enhancement that could reduce injection variability.[101]

Working with animals introduces many uncertainties without introducing any human error, but that must be considered as well. Although conditions were similar from one experimental trial to the next, various other factors could have impacted the results. Among these effects are: timing, lighting, temperature, and GTNO application differences.

During data analysis several consistent assumptions were chosen arbitrarily. These included the 10%, 20% and 50% standards of intensity return for determination of pumping pressure and the power of the FFT when determining packet restoration. The determined pressure difference between control and treatment cases as determined by the 10% restoration of flow metric was the only one of the four methods that was not statistically significant. The intensity values of some trials showed increases in intensity even during complete flow occlusion at 80 mmHg. It is possible that some lymph fluid including ICG dye diffused through a luminal opening in the vessel created during its non-uniform collapsing during pressure application. This may have resulted in the determination of 80 mmHg for several of the trials when the 10% metric was used. For that reason, this is probably not the most accurate method of pressure determination. Because the 50% flow restoration metric yielded pressure values that most immolated those determined by the packet restoration metric of measurement, it is suggested that it is the most accurate of the percentage metrics of pressure determination. Because these analysis processes were automated they did not leave any room for simple experimental observation. Determination of flow restoration by the three volunteer lab members was highly subjective and variable, but also resulted in statistically significant differences between the control and treatment cases. The average values between the control and

treatment cases were closest for the lab member average metric of pressure determination. It is fitting that many of the values determined during the automated analysis were fairly consistent with those visually confirmed during the experiments. Despite all of the uncertainties and assumptions involved in the process, the results definitively showed a significant difference between the treatment (GTNO) and control case.

The method used to measure these pressures was not necessarily optimized. Future studies should not rely on the established pressure curve as if it is the gold standard. It was developed through many trials with intentionality, but may have some weaknesses. Although 80 mmHg was around reported values of diastolic blood pressure in rats, this does not take into account the anesthetics used in this study, the effects of which were not known during the development of the pressure curve. Even if 80 mmHg was low enough that it did not occlude blood flow, it may have had a negative effect on venous return that was not considered. Additionally, there was also flow return indicated on the intensity plots of several trials during complete occlusion at 80 mmHg. As previously discussed, this may not be due completely to lymphangion contractions upstream. However, in future studies it may not be as beneficial as initially assumed to skip decrements in pressure between 80 mmHg and 55mmHg, because there is a chance that flow restoration could have occurred at a pressure between the two. Also, to reduce the amount of time that the vessel was occluded, with the hopes of damping effects of prolonged occlusion, the pressure was only held at each value for one minute. Findings could be different if this hold time was increased, particularly for the treatment cases in which pump function was already noticeably reduced, resulting in higher pressure

determinations. Perhaps the hold time could be proportionally increased for the treatment case to reflect the increase in transport time. Although the standardized pressure curve may have had some weaknesses, many more trials would need to be performed to optimize it. For this study it was sufficient for elucidating valuable information about the effects of nitric oxide application on the lymphatic system.

CHAPTER 3

CONCLUSION AND FUTURE WORK

Motivated by a significant need for minimally invasive methods for quantifying nitric oxide effects on lymphatic function in vivo, a pressure cuff system was designed and used in conjunction with an established NIR imaging system to measure differences in lymphatic pumping pressure upon dermal delivery of NO. Thus, the sensitivity of the pressure cuff system was also demonstrated. The system exhibited closed-loop feedback control with strong steady-state tracking ability and automation of the pressure application curve for repeatability and precision. Integrated image processing techniques allowed for quantification of lymphatic pumping pressure from NIR image sequences taken during cuff deflation. To show the functionality of such a system it was demonstrated for the first time *in vivo* that dermally delivered nitric oxide causes a significant reduction in lymphatic pumping pressure. The ability to measure lymphatic pumping pressure non-invasively has the potential to significantly enhance attempts to obtain actual functional data on lymphatic physiology *in vivo*. Additionally, implementation of the advances reported here holds strong potential for the clinical early detection and diagnosis of lymphedema.

Applying these techniques to the study of rodent lymphatic vasculature has opened the door for future *in vivo*, non-invasive, molecular studies on the regulation of lymphatic pumping, such as investigation of how nitric oxide serves to regulate pumping pressure in physiologic and pathophysiologic contexts. The simple geometry and anatomy of the lymphatic vessels in the rodent tail make this is an ideal place to measure pumping pressure. Also, the rodent tail is one of the most developed animal models of

lymphedema,[84,86-88,102,103] where the addition of this tool set could provide remarkable insight into lymphedema progression and pathology.

If it could be demonstrated on a rodent model that the fabricated system can detect lymphatic pumping pressure differences throughout disease progression, then it is suggested that such a procedure could be scaled up for use on humans. The eventual goal would be to produce a clinical diagnostic tool for lymphatic disorders that could detect early onset of disease. That way treatment could be administered before long-term irreversible damage was done.

The demonstrated sensitivity of the system to measuring difference in pumping pressure after the application of the GTNO ointment suggests that the effects of other vasoactive substances on pumping pressure may also be determinable. Some of the vasoactive substances that have been shown to increase phasic contractions are endothelin-1, norepinephrine, and thromboxane-A2 analog U-46619.[29] If progression of lymphatic disease is shown to correlate with reduction in pumping pressure, and a substance is demonstrated to increase lymphatic vessel contractility, and therefore pumping pressure, then treatment of lymphatic disease could be well on its way. This project and study hold potential for multiple applications of continued research that could positively enhance the search for lymphatic disorder diagnostics and treatments.

REFERENCES

1. Browse SN, Burnand KG, Mortimer PS. *Diseases of the Lymphatics*. London: Arnold; 2003:1–18.

2. Rockson SG. Diagnosis and Management of Lymphatic Vascular Disease. *Journal of the American College of Cardiology*. 2008;52(10):799–806.

3. Glisson F. *Anatomia hepatis*. London, England: DuGardionis; 1654.

4. Cruikshank WC. *The anatomy of the absorbing vessels of the human body*. London: G. Nicol; 1786.

5. Dongaonkar RM, Laine GA, Stewart RH, Quick CM. Balance point characterization of interstitial fluid volume regulation. *AJP: Regulatory, Integrative and Comparative Physiology*. 2009;297(1):R6–R16.

6. Nipper ME, Dixon JB. Engineering the Lymphatic System. *Cardiovascular Engineering and Technology*. 2011;2:296–308.

7. Paolo M. *Vasorum lymphaticorum corporis humani historia et ichnographia auctore Paulo Mascagni.*; 1787.

8. Liao S, Cheng G, Conner DA, Huang Y, Kucherlapati RS, Munn LL, Ruddle NH, Jain RK, Fukumura D, Padera TP. Impaired lymphatic contraction associated with immunosuppression. *Proc Natl Acad Sci*. 2011;108:18784–18789.

9. Randolph GJ, Angeli V, Swartz MA. Dendritic-cell trafficking to lymph nodes through lymphatic vessels. *Nature Reviews Immunology*. 2005;5(8):617–628.

10. Dixon JB. Lymphatic lipid transport: sewer or subway? *Trends in Endocrinology & Metabolism*. 2010;21:480–487.

11. Lund AW, Swartz MA. Role of Lymphatic Vessels in Tumor Immunity: Passive Conduits or Active Participants? *Journal of Mammary Gland Biology and Neoplasia*. 2010;15(3):341–352.

12. Kajiya K, Kidoya H, Sawane M, Matsumoto-Okazaki Y, Yamanishi H, Furuse M, Takakura N. Promotion of Lymphatic Integrity by Angiopoietin-1/Tie2 Signaling during Inflammation. *AJPA*. 2012;180(3):1273–1282.

13. Arnold R, Ashwell K, Bryce D, al E. *The Encyclopedic Atlas to the Human*

Body. NSW, Australia: Global Book Publishers; 2004:55–57.

14. Schmid-Schonbein GW. Microlymphatics and lymph flow. *Physiol Rev*. 1990;70(4):987–1028.

15. Negrini D, Moriondo A. Lymphatic anatomy and biomechanics. *The Journal of Physiology*. 2011;589(12):2927–2934.

16. Hunter W. *Hunter's lectures of anatomy*. London: Elsevier; 1972.

17. Galie P, Spilker RL. A Two-Dimensional Computational Model of Lymph Transport Across Primary Lymphatic Valves. *Journal of Biomechanical Engineering*. 2009;131(11):111004.

18. Leak LV. Studies on the permeability of lymphatic capillaries. *The Journal of Cell Biology*. 1971;50(2):300–323.

19. Keene DR, Sakai LY, Lunstrum GP, Morris NP, Burgeson RE. Type VII collagen forms an extended network of anchoring fibrils. *J Cell Biol*. 1987;104(3):611–621.

20. Chen M, Marinkovich MP, Veis A, Cai X, Rao CN, O'Toole EA, Woodley DT. Interactions of the amino-terminal noncollagenous (NC1) domain of type VII collagen with extracellular matrix components. *Journal of Biological Chemistry*. 1997;272(23):14516–14522.

21. Castenholz A. Structural and functional properties of initial lymphatics in the rat tongue. *Lymphology*. 1987;20(3):112–125.

22. Casley-Smith JR, FLOREY HW. The structure of normal small lymphatics. *Experimental Physiology*. 1961;46(1):101–106.

23. Ohhashi T, Azuma T, Sakaguchi M. Active and passive mechanical characteristics of bovine mesenteric lymphatics. *Heart and Circulatory Physiology*. 1980;239(1):88–95.

24. Alitalo K, Tammela T, Petrova TV. Lymphangiogenesis in development and human disease. *Nature*. 2005;438(7070):946–953.

25. Levick JR, Michel CC. Microvascular fluid exchange and the revised Starling principle. *Cardiovascular Research*. 2010;87(2):198–210.

26. Gashev AA. Lymphatic Vessels: Pressure- and Flow-dependent Regulatory Reactions. *Annals of the New York Academy of Sciences*. 2008;1131(1):100–109.

27. Weid von der P-Y, Zawieja DC. Lymphatic smooth muscle: the motor unit of

lymph drainage. *The International Journal of Biochemistry & Cell Biology*. 2004;36(7):1147–1153.

28. Muthuchamy M. Molecular and functional analyses of the contractile apparatus in lymphatic muscle. *The FASEB Journal*. 2003;17:920–922.

29. Telinius N, Drewsen N, Pilegaard H, Kold-Petersen H, de Leval M, Aalkjaer C, Hjortdal V, Boedtkjer DB. Human thoracic duct in vitro: diameter-tension properties, spontaneous and evoked contractile activity. *AJP: Heart and Circulatory Physiology*. 2010;299(3):H811–H818.

30. Bohlen HG, Wang W, Gashev A, Gasheva O, Zawieja D. Phasic contractions of rat mesenteric lymphatics increase basal and phasic nitric oxide generation in vivo. *AJP: Heart and Circulatory Physiology*. 2009;297(4):H1319–H1328.

31. Mizuno R, Koller A, Kaley G. Regulation of the vasomotor activity of lymph microvesselsby nitric oxide and prostaglandins. *Am J Physiol Regul Integr Comp Physiol*. 1998;274:R790–R796.

32. Weiler M, Kassis T, Dixon JB. Sensitivity analysis of near-infrared functional lymphatic imaging. *Journal of Biomedical Optics*. 2012;17(6):066019:1–11.

33. Gashev AA. Inhibition of the active lymph pump by flow in rat mesenteric lymphatics and thoracic duct. *The Journal of Physiology*. 2002;540(3):1023–1037.

34. Saul ME, Thomas PA, Dosen PJ, Isbister GK, O'Leary MA, Whyte IM, McFadden SA, van Helden DF. A pharmacological approach to first aid treatment for snakebite. *Nature Medicine*. 2011;17(7):809–811.

35. Bohlen HG, Gasheva OY, Zawieja DC. Nitric oxide formation by lymphatic bulb and valves is a major regulatory component of lymphatic pumping. *AJP: Heart and Circulatory Physiology*. 2011;301(5):H1897–H1906.

36. Tsunemoto H, Ikomi F, Ohhashi T. Flow-mediated release of nitric oxide from lymphatic endothelial cells of pressurized canine thoracic duct. *The Japanese journal of physiology*. 2003;53(3):157–163.

37. Radhakrishnan K, Rockson SG. The Clinical Spectrum of Lymphatic Disease. *Annals of the New York Academy of Sciences*. 2008;1131(1):155–184.

38. Rockson SG. Lymphedema. *Am J Med*. 2001;110:288–295.

39. Rockson SA. Lymphedema: anatomy, physiology and pathogenesis. 1997;2(4):321–326.

40. Browse NL, Stewart G. Lymphedema: pathophysiology and classification. *The Journal of Cardiovascular Surgery*. 1985;26(2):91–106.

41. Rockson SG, Rivera KK. Estimating the Population Burden of Lymphedema. *Annals of the New York Academy of Sciences*. 2008;1131(1):147–154.

42. Stanton AWB, Modi S, Mellor RH, Levick JR, Mortimer PS. Recent Advances in Breast Cancer-Related Lymphedema of the Arm: Lymphatic Pump Failure and Predisposing Factors. *Lymphatic Research and Biology*. 2009;7(1):29–45.

43. Tobin MB, Lacey HJ, Meyer L, Mortimer PS. The psychological morbidity of breast cancer–related arm swelling. Psychological morbidity of lymphoedema. *Cancer*. 2006;72(11):3248–3252.

44. Tiwari A, Myint F, Hamilton G. Management of Lower Limb Lymphoedema in the United Kingdom. *European Journal of Vascular and Endovascular Surgery*. 2006;31(3):311–315.

45. Benoit JN, Zawieja DC, Goodman AH, Granger HJ. Characterization of intact mesenteric lymphatic pump and its responsiveness to acute edemagenic stress. *AJP: Heart and Circulatory Physiology*. 1989;257(6):2059–2069.

46. Deakin CD, Low JL. Accuracy of the advanced trauma life support guidelines for predicting systolic blood pressure using carotid, femoral, and radial pulses: observational study. *Bmj*. 2000;321(7262):673–674.

47. Garcia JN, Pedersen NP, Nalivaiko E, Blessing WW. Tail artery blood flow measured by chronically implanted Doppler ultrasonic probes in unrestrained conscious rats. *Journal of neuroscience methods*. 2001;104(2):209–213.

48. Moniz E. L'encéphalographie artérielle, son importance dans la localisation des tumeurs cérébrales. *Reviews of Neurology*. 1927;2(1):72.

49. Hudack SS, McMaster PD. The Lyphatic Participation In Human Cutaneous Phenomena a Study of the Minute Lymphatics of the Living Skin. *The Journal of experimental medicine*. 1933;57(5):751–774.

50. Glenn WWL. The Lymphatic System. *Archives of Surgery*. 1981;116(8):989–995.

51. Kinmonth JB. Lymphangiography in man. *Clinical Science*. 1952;(11):13–20.

52. Clement O, Luciani A. Imaging the lymphatic system: possibilities and clinical applications. *European Radiology*. 2004;14(8).

53. Moghimi SM, Bonnemain B. Subcutaneous and intravenous delivery of

diagnostic agents to the lymphatic system: applications in lymphoscintigraphy and indirect lymphography. *Advanced Drug Delivery Reviews*. 1999;37(1):295–312.

54. Witte CL, Witte MH. Diagnostic and interventional imaging of lymphatic disorders. *International Angiology*. 1999;18(1):25–30.

55. Weissleder R, Elizondo G, Josephson L, Compton CC, Fretz CJ, Stark DD, Ferrucci JT. Experimental lymph node metastases: enhanced detection with MR lymphography. *Radiology*. 1989:835–839.

56. Weissleder R, Elizondo G, Wittenberg J, Rabito CA, Bengele HH, Josephson L. Ultrasmall superparamagnetic iron oxide: characterization of a new class of contrast agents for MR imaging. *Radiology*. 1990:489–493.

57. Sharma R, Wendt JA, Rasmussen JC, Adams KE, Marshall MV, Sevick-Muraca EM. New Horizons for Imaging Lymphatic Function. *Annals of the New York Academy of Sciences*. 2008;1131(1):13–36.

58. Suresh S, Kumaraswami V, Suresh I, Rajesh K, Suguna G, Vijayasekaran V, Ruckmani A, Rajamanickam MG. Ultrasonographic diagnosis of subclinical filariasis. *Journal of Ultrasound in Medicine*. 1997;16:45–49.

59. Dayton PA, Rychak JJ. Molecular ultrasound imaging using microbubble contrast agents. *Front Biosci*. 2007;12(23):5124–5142.

60. Byron B, Ernst LA, Waggoner AS. Fluorescence imaging of tumors in vivo. *Current medicinal chemistry*. 2005;12(7):795–805.

61. Rao J, Dragulescu-Andrasi A, Yao H. Fluorescence imaging in vivo: recent advances. *Current Opinion in Biotechnology*. 2007;18(1):17–25.

62. Frangioni J. In vivo near-infrared fluorescence imaging. *Current Opinion in Chemical Biology*. 2003;7(5):626–634.

63. Sharma R, Wang W, Rasmussen JC, Joshi A, Houston JP, Adams KE, Cameron A, Ke S, Kwon S, Mawad ME, Sevick-Muraca EM. Quantitative imaging of lymph function. *AJP: Heart and Circulatory Physiology*. 2007;292(6):H3109–H3118.

64. Kwon S, Sevick-Muraca EM. Noninvasive Quantitative Imaging of Lymph Function in Mice. *Lymphatic Research and Biology*. 2007;5(4):219–232.

65. Sevick-Muraca EM, Sharma R, Rasmussen JC, Marshall MV, Wendt JA, Pham HQ, Bonefas E, Houston JP, Sampath L, Adams KE, Blanchard DK, Fisher RE, Chiang SB, Elledge R, Mawad ME. Imaging of Lymph Flow in Breast Cancer

Patients after Microdose Administration of a Near-Infrared Fluorophore: Feasibility Study. *Radiology*. 2008;246(3):734–741.

66. Gurfinkel M, Thompson AB, Ralston W, Troy TL, Moore AL, Moore TA, Gust JD, Tatman D, Reynolds JS, Muggenburg B. Pharmacokinetics of ICG and HPPH-car for the Detection of Normal and Tumor Tissue Using Fluorescence, Near-infrared Reflectance Imaging: A Case Study¶. *Photochemistry and photobiology*. 2000;72(1):94–102.

67. Kitai T, Inomoto T, Miwa M, Shikayama T. Fluorescence navigation with indocyanine green for detecting sentinel lymph nodes in breast cancer. *Breast Cancer*. 2005;12(3):211–215.

68. Unno N, Inuzuka K, Suzuki M, Yamamoto N, Sagara D, Nishiyama M, Konno H. Preliminary experience with a novel fluorescence lymphography using indocyanine green in patients with secondary lymphedema. *Journal of Vascular Surgery*. 2007;45(5):1016–1021.

69. Unno N, Tanaka H, Suzuki M, Yamamoto N, Mano Y, Sano M, Saito T, Konno H. Influence of age and gender on human lymphatic pumping pressure in the leg copy. *Lymphology*. 2012:113–120.

70. Unno N, Nishiyama M, Suzuki M, Tanaka H, Yamamoto N, Sagara D, Mano Y, Konno H. A novel method of measuring human lymphatic pumping using indocyanine green fluorescence lymphography. *Journal of Vascular Surgery*. 2010;52(4):946–952.

71. Alitalo K, Carmeliet P. Molecular mechanisms of lymphangiogenesis in health and disease. *Cancer cell*. 2002;1(3):219–227.

72. Hagendoorn J. Endothelial Nitric Oxide Synthase Regulates Microlymphatic Flow via Collecting Lymphatics. *Circulation Research*. 2004;95(2):204–209.

73. Gasheva OY, Zawieja DC, Gashev AA. Contraction-initiated NO-dependent lymphatic relaxation: a self-regulatory mechanism in rat thoracic duct. *The Journal of Physiology*. 2006;575(3):821–832.

74. Ribera J, Pauta M, Melgar-Lesmes P, Tugues S, Fernández-Varo G, Held KF, Soria G, Tudela R, Planas AM, Fernández-Hernando C, Arroyo V, Jiménez W, Morales-Ruiz M. Increased nitric oxide production in lymphatic endothelial cells causes impairment of lymphatic drainage in cirrhotic rats. *Gut*. 2011.

75. Akl TJ, Nagai T, Cote GL, Gashev AA. Mesenteric lymph flow in adult and aged rats. *AJP: Heart and Circulatory Physiology*. 2011;301(5):H1828–H1840.

76. Jensen LDE, Cao R, Hedlund EM, Söll I, Lundberg JO, Hauptmann G,

Steffensen JF, Cao Y. Nitric oxide permits hypoxia-induced lymphatic perfusion by controlling arterial-lymphatic conduits in zebrafish and glass catfish. *Proceedings of the National Academy of Sciences*. 2009;106(43):18408–18413.

77. Lahdenranta J, Hagendoorn J, Padera TP, Hoshida T, Nelson G, Kashiwagi S, Jain RK, Fukumura D. Endothelial Nitric Oxide Synthase Mediates Lymphangiogenesis and Lymphatic Metastasis. *Cancer Research*. 2009;69(7):2801–2808.

78. Mihara M, Hara H, Hayashi Y, Narushima M, Yamamoto T, Todokoro T, Iida T, Sawamoto N, Araki J, Kikuchi K, Murai N, Okitsu T, Kisu I, Koshima I. Pathological Steps of Cancer-Related Lymphedema: Histological Changes in the Collecting Lymphatic Vessels after Lymphadenectomy. Greene A, ed. *PLoS ONE*. 2012;7(7):e41126:1–10.

79. Lim HY, Rutkowski JM, Helft J, Reddy ST, Swartz MA, Randolph GJ, Angeli V. Hypercholesterolemic Mice Exhibit Lymphatic Vessel Dysfunction and Degeneration. *The American Journal of Pathology*. 2009;175(3):1328–1337.

80. Hargens AR, Zweifach BW. Contractile stimuli in collecting lymph vessels. *American Journal of Physiology-Heart and Circulatory Physiology*. 1977;233(1):H57–H65.

81. Leu AJ, Berk DA, Yuan F, Jain RK. Flow velocity in the superficial lymphatic network of the mouse tail. *AJP: Heart and Circulatory Physiology*. 1994;267(4):H1507–H1513.

82. Yoon Y-S, Murayama T, Gravereaux E, Tkebuchava T, Silver M, Curry C, Wecker A, Kirchmair R, Hu CS, Kearney M, Ashare A, Jackson DG, Kubo H, Isner JM, Losordo DW. VEGF-C gene therapy augments postnatal lymphangiogenesis and ameliorates secondary lymphedema. *Journal of Clinical Investigation*. 2003;111(5):717–725.

83. Boardman KC. Interstitial Flow as a Guide for Lymphangiogenesis. *Circulation Research*. 2003;92(7):801–808.

84. Goldman J, Conley KA, Raehl A, Bondy DM, Pytowski B, Swartz MA, Rutkowski JM, Jaroch DB, Ongstad EL. Regulation of lymphatic capillary regeneration by interstitial flow in skin. *AJP: Heart and Circulatory Physiology*. 2007;292(5):H2176–H2183.

85. Clavin NW, Avraham T, Fernandez J, Daluvoy SV, Soares MA, Chaudhry A, Mehrara BJ. TGF- 1 is a negative regulator of lymphatic regeneration during wound repair. *AJP: Heart and Circulatory Physiology*. 2008;295(5):H2113–H2127.

86. Rutkowski JM, Moya M, Johannes J, Goldman J, Swartz MA. Secondary lymphedema in the mouse tail: Lymphatic hyperplasia, VEGF-C upregulation, and the protective role of MMP-9. *Microvascular Research*. 2006;72(3):161–171.

87. Tabibiazar R, Cheung L, Han J, Swanson J, Beilhack A, An A, Dadras SS, Rockson N, Joshi S, Wagner R, Rockson SG. Inflammatory Manifestations of Experimental Lymphatic Insufficiency. *PLoS Medicine*. 2006;3(7):e254:1114–1139.

88. Zampell JC, Elhadad S, Avraham T, Weitman E, Aschen S, Yan A, Mehrara BJ. Toll-like receptor deficiency worsens inflammation and lymphedema after lymphatic injury. *AJP: Cell Physiology*. 2012;302(4):C709–C719.

89. Rasmussen JC, Tan I-C, Marshall MV, Fife CE, Sevick-Muraca EM. Lymphatic imaging in humans with near-infrared fluorescence. *Current Opinion in Biotechnology*. 2009;20(1):74–82.

90. Mihara M, Hara H, Araki J, Kikuchi K, Narushima M, Yamamoto T, Iida T, Yoshimatsu H, Murai N, Mitsui K, Okitsu T, Koshima I. Indocyanine Green (ICG) Lymphography Is Superior to Lymphoscintigraphy for Diagnostic Imaging of Early Lymphedema of the Upper Limbs. Gelovani JG, ed. *PLoS ONE*. 2012;7(6):e38182:1–9.

91. Barrett T, Choyke PL, Kobayashi H. Imaging of the lymphatic system: new horizons. *Contrast Media & Molecular Imaging*. 2006;1(6):230–245.

92. Misselwitz B. MR contrast agents in lymph node imaging. *European Journal of Radiology*. 2006;58(3):375–382.

93. Tammela T, Alitalo K. Lymphangiogenesis: Molecular Mechanisms and Future Promise. *Cell*. 2010;140(4):460–476.

94. Kassis T, Kohan AB, Weiler MJ, Nipper ME, Cornelius R, Tso P, Dixon JB. Dual-channel in-situ optical imaging system for quantifying lipid uptake and lymphatic pump function. *Journal of Biomedical Optics*. 2012;17(8):086005–1–086005–13.

95. Modi S, Stanton AWB, Svensson WE, Peters AM, Mortimer PS, Levick JR. Human lymphatic pumping measured in healthy and lymphoedematous arms by lymphatic congestion lymphoscintigraphy. *The Journal of Physiology*. 2007;583(1):271–285.

96. Bunag RD, Butterfield J. Tail-cuff blood pressure measurement without external preheating in awake rats. *Hypertension*. 1982;4(6):898–903.

97. Byrom FB, Wilson C. A plethysmographic method for measuring systolic blood pressure in the intact rat. *The Journal of Physiology*. 1938;93(3):301–304.

98. Olszewski WL, Engeset A. Intrinsic contractility of prenodal lymph vessels and lymph flow in human leg. *American Journal of Physiology-Heart and Circulatory Physiology*. 1980;239(6):H775–H783.

99. Rees DD, Palmer RM, Moncada S. Role of endothelium-derived nitric oxide in the regulation of blood pressure. *Proceedings of the National Academy of Sciences*. 1989;86(9):3375–3378.

100. Rumbaut RE, McKay MK, Huxley VH. Capillary hydraulic conductivity is decreased by nitric oxide synthase inhibition. *American Journal of Physiology-Heart and Circulatory Physiology*. 1995;268:H1856–H1861.

101. Gupta J, Felner EI, Prausnitz MR. Minimally Invasive Insulin Delivery in Subjects with Type 1 Diabetes Using Hollow Microneedles. *Diabetes Technology & Therapeutics*. 2009;11:329–337.

102. Aschen S, Zampell JC, Elhadad S, Weitman E, De Brot M, Mehrara BJ. Regulation of Adipogenesis by Lymphatic Fluid Stasis. *Plastic and Reconstructive Surgery*. 2012;129(4):838–847.

103. Wu X, Zhuo S, Chen J, Liu N. Real-time in vivo imaging collagen in lymphedematous skin using multiphoton microscopy. *Scanning*. 2011;33(6):463–467.

APPENDIX A

LOG OF RATS USED THROUGHOUT THE STUDY

Table A.1 Log of Rats Used Throughout the Study. This Table shows the relevant information for all rat trials conducted throughout this project. The rats used for data collection for the paper in Chapter 2 are highlighted. Wherever cells are blank there was either no definitive value for that column or it was not collected at the time of the trial. Many advances were made in the computer program, controls, injections, and other methods throughout the earlier trials. The effectiveness of these advances is exhibited in the successful trials conducted in the highlighted region, where data was used in the paper submitted for publication.

Rat Number	Gender	DOB	Date of Use	Age (days)	Weight at use	Cuff size	Frame Started	Pressure	Nair	GTNO	Result
1	F		4/6/12		308	L	270, 1355	~30	No	No	first trial, flow stopped and restored
2	M	3/16/12	5/18/12	63	180	M	460	~45	No	No	poor packet flow
3	M	3/16/12	5/24/12	69	290	M	120	40	No	No	good trial
4	F	3/30/12	6/8/12	70	200	M	~8	25	No	No	good trial
5	F	3/30/12	6/11/12	73	210	M			No	No	fail: computer program
6	F	3/23/12	6/14/12	83	370	M	815		No	No	camera malfunctioning, no flow ever established
7	F	3/23/12	6/14/12	83	335	M	30		No	No	intensity too low to detect any differences, made new ICG, failed attempt
8	F	4/6/12	6/27/12	82	225	M	205	22	No	No	good trial
9	M	4/20/12	7/2/12	73	300	M	730	~38	No	No	no intesnity indication of returned flow
10	M	4/20/12	7/2/12	73	340	M			No	No	failed, no changes in intesity
11	M	4/20/12	7/12/12	83	365	L	400	~30	No	No	good trial
12	M	4/20/12	7/12/12	83	335	L	250, 300	32.5	No	No	good trial
13	M	4/27/12	7/19/12	83	340	M	200	37.5	Yes	No	good trial, different pressures for each vessel ROI1 and ROI2
14	M	4/27/12	7/19/12	83	355	M	200	37.5 & 30	Yes	No	good trial, different pressures for each vessel ROI1 and ROI2
15	M	5/1/12	7/20/12	80	312.3	M	200	50	Yes	No	still flow at crazy high pressures (even up at >80 mmHg in both vessels I think)
16	M	5/1/12	7/20/12	80	303.6	M	255	27.5	Yes	No	drastic difference in ROI1 and ROI2
17	M	5/25/12	7/26/12	62	250	M	230	27.5	Yes	No	drastic difference in ROI1 and ROI2
18	M	5/25/12	7/26/12	62	240	M	230	32.5	Yes	No	drastic difference in ROI1 and ROI2
19	M	5/25/12	7/27/12	63	246	M	510	17.5	Yes	Yes	drastic difference in ROI1 and ROI2
20	M	5/25/12	7/27/12	63	250.5	M	105	17.5	Yes	Yes	drastic difference in ROI1 and ROI2
21	M	6/1/12	8/1/12	61	252.4	M	300	~27.5	Yes	Yes	not as much oitment on this one
22	M	6/1/12	8/1/12	61	258.9	M	400	~5	Yes	Yes	lots of ointment on this one
23	M	6/1/12	8/2/12	62	292.5	M	500	37.5 or 10	Yes	Yes	lights on/off throughout procedure...difficult to tell
24	M	6/1/12	8/2/12	62	239.9	M	730	22.5-25	Yes	Yes	Great intensity plots
25	M	6/8/12	8/9/12	62	273	M	500	32.5	Yes	No	gradual increase in intensity - weaker flow in bottom (left) vessel
26	M	6/8/12	8/9/12	62	250.8	M	360	40	Yes	No	tail shifted a little, motion compensation required, decent trial
27	M	6/15/12	8/16/12	62	263.4	M	300	35	Yes	No	shutter issues, great flow in bottom vessel, flow verified with video post-experiment in Fuji
28	M	6/15/12	8/16/12	62	224	M	390	55	Yes	No	poor injection, shutter issues galore, packets returned super early I think, no comprendo
29	M	6/15/12	-	-	-	-	-	-	Yes	-	never used due to shutter malfunctions
30	M	6/15/12	-	-	-	-	-	-	Yes	-	never used due to shutter malfunctions

APPENDIX B

INTENSITY PLOTS FOR RATS INCLUDED IN CHAPTER 2

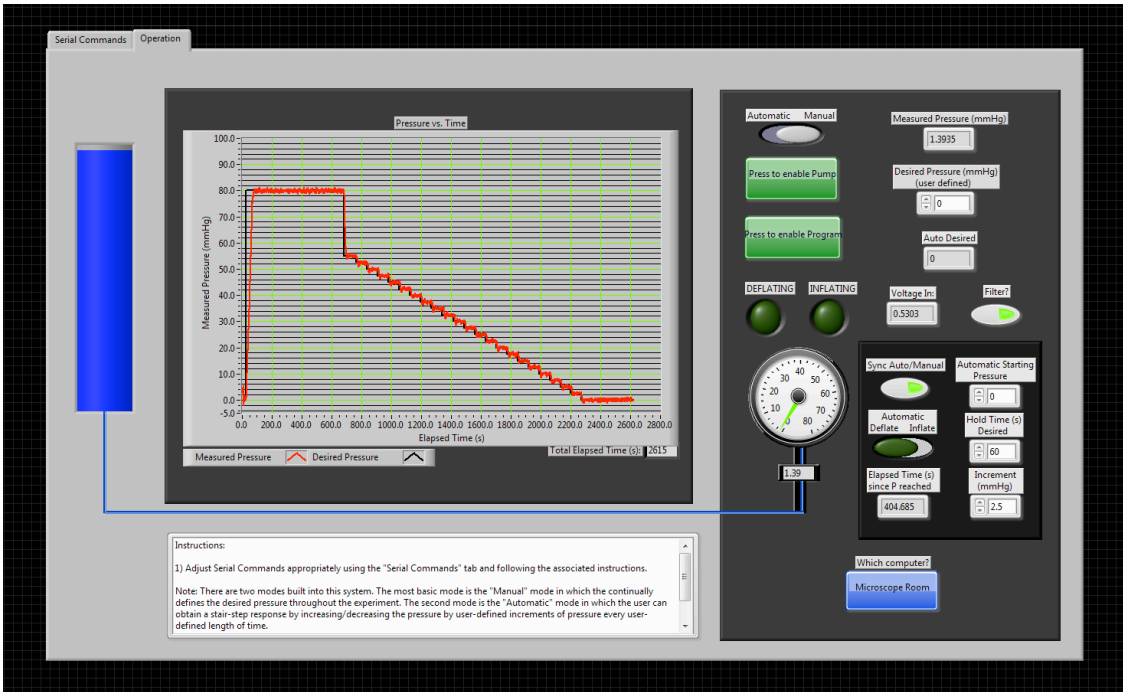

Figure B.1 Pressure Cuff Program GUI. This is a screenshot of the pressure cuff program graphical user interface (GUI) after completion one representative experiment. It shows the standard pressure curve used for all of the subsequent experiments for which the Intensity plots are shown.

Note: The first “Rat #” correlates to that for the experiments included in the paper in Chapter 2 (colored in Appendix A), and the one in parenthesis correlates to the overall number of all rats tested (see all of Appendix A).

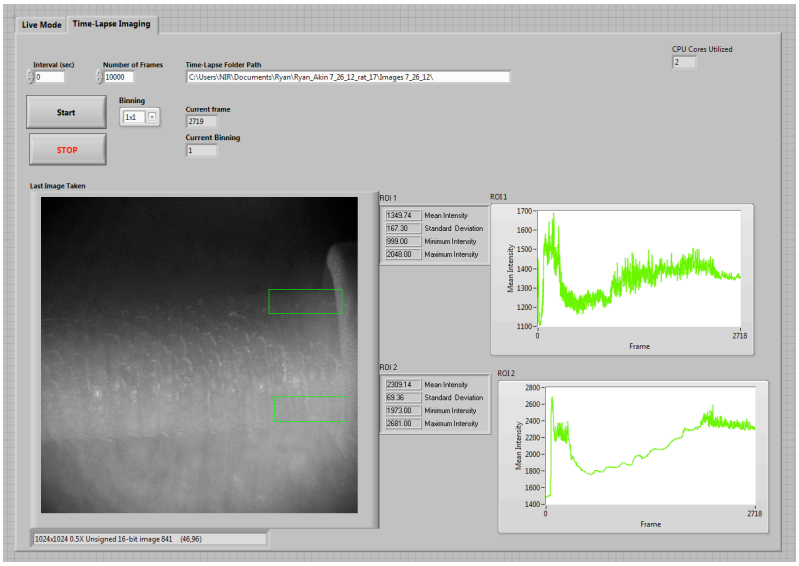

Figure B.2 Rat 1 (Rat 17 – 7/26/12): A strange glare appeared over ROI1 throughout the experiment, which is evidenced by the unusual noise in the intensity plot. It was eventually deduced that this glare was due to issues with timing of the shutter of the camera, which was subsequently replaced. ICG clearance occurred quickly after inflation of the cuff, which is evidenced by the large drop in intensity in each ROI. Packet restoration could be detected in ROI2 at 27.5 mmHg followed by much more obvious packet flow at 17.5 mmHg.

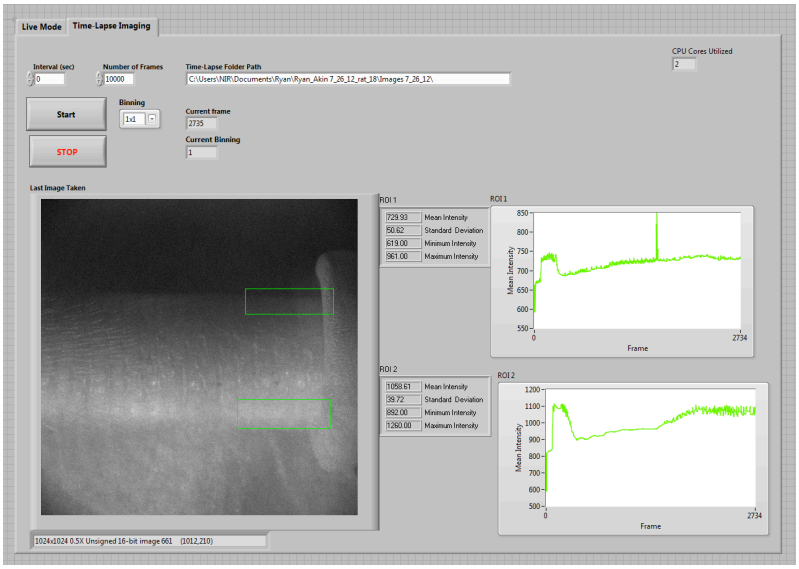

Figure B.3 Rat 2 (Rat 18 – 7/26/12): Flow appeared to be restored in ROI1 around 55 mmHg. Slight packet flow returned in ROI2 at 40 mmHg, but it was difficult to see. More obvious confirmation of packet flow was made at 32.5 mmHg. During this trial it was discovered that the ROIs eclipsed the pressure cuff, which likely impacted the intensity plots during inflation/deflation of the cuff.

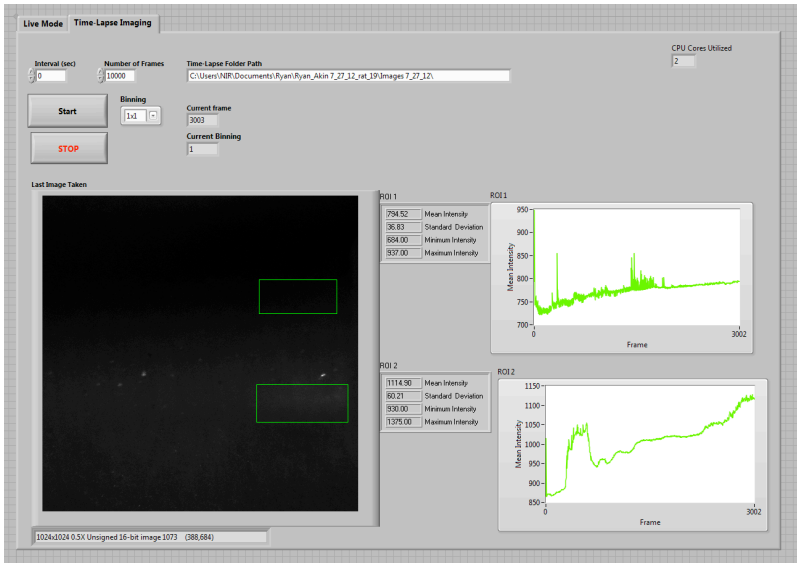

Figure B.4 Rat 3 (Rat 19 – 7/27/12): The darkness of the image was due to bright spots on the tail and normalization of the image to them. This occurred in the GTNO cases for some reason and attempts were made to cover the spot, thereby reducing the contrast between the darkest and brightest areas of the image. GTNO ointment was applied to the entire tail. The injection was poor and required several more pokes of the needle and slight massage proximal to the initial injection to induce flow. Flow was much slower as anticipated for the GTNO cases. Packet flow was visually confirmed around 20-17.5 mmHg. To reduce the bright spots, likely specks of ICG, gloves were changed before application of GTNO. Some ICG could have been transferred to the gloves during filling of the syringe with ICG, then to the tail during GTNO application.

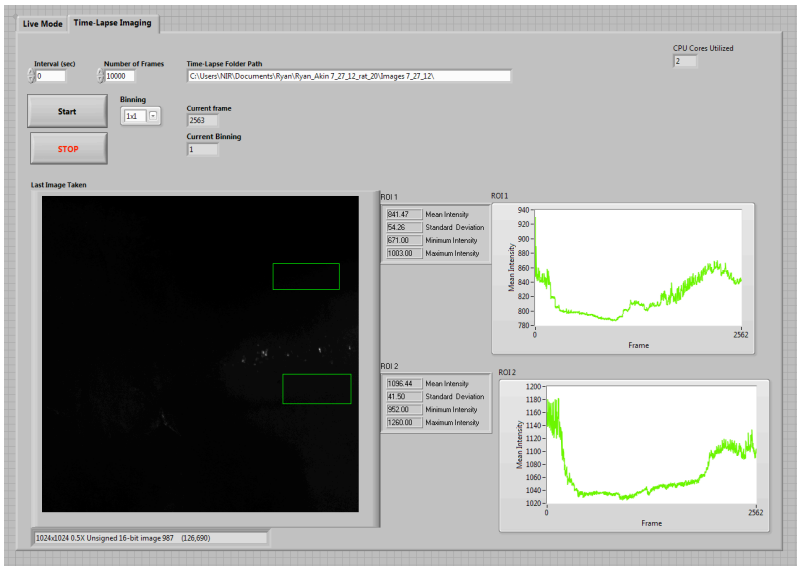

Figure B.5 Rat 4 (Rat 20 – 7/27/12): Another dark image, with little evidence of the cause. ROI1 intensity jumped around 45 mmHg, while ROI2 intensity jumped at 20 mmHg. Flow in ROI2 became more visible when the pressure was decreased from 17.5 mmHg to 15 mmHg.

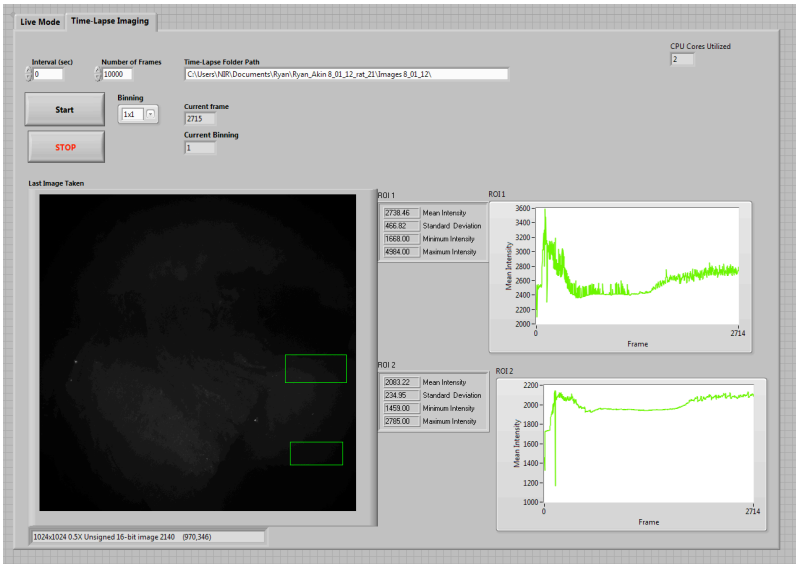

Figure B.6 Rat 5 (Rat 21 – 8/1/12): Packets were visible in ROI2 before inflation and after deflation. Once again, shutter problems cause an intermittent glare that produced significant noise in the ROI1 intensity. The bright spots in this image sequence were covered with a non-fluorescent piece of plastic to increase visualization of flow. Flow through ROI1 appeared to return around 35 mmHg, and flow in ROI2 around 27.5 mmHg. Packets were definitely visible at 22.5 mmHg. Not as much ointment was placed on the tail of this one as on the previous rat.

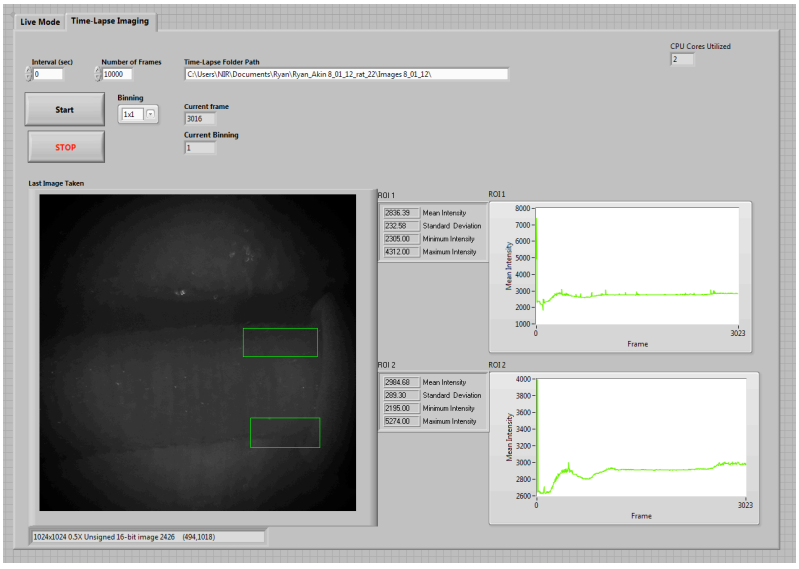

Figure B.7 Rat 6 (Rat 22 – 8/1/12): A lot of GTNO ointment was applied. For some reason the tail was twitching after anesthetization. A possible increase in intensity was seen at around 15 mmHg. A more obvious increase was witnessed at around 5 mmHg in ROI2.

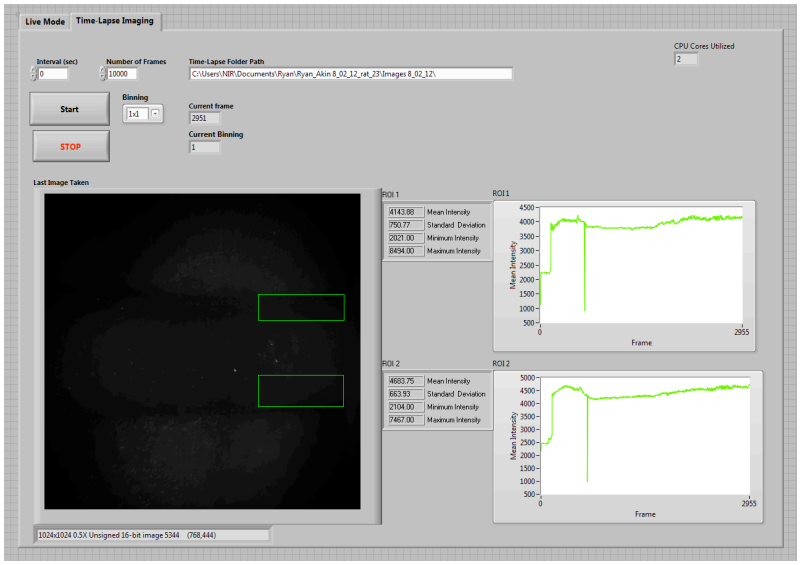

Figure B.8 Rat 7 (Rat 23 – 8/2/12): Before this trial the elastic thin tubing inflatable bladder was replaced. The thin spike was due to adjustment of the laser placement. This trial produced the best images of a treatment (GTNO) tail to this point. The camera and laser were on for a while before the start of the trial. It took a long time for packet flow to appear. It was difficult to tell when intensity of ICG rose in ROI2, but it may have been around 37.5 mmHg or as low as 10 mmHg. Flow in ROI1 appeared to be restored at around 37.5 mmHg.

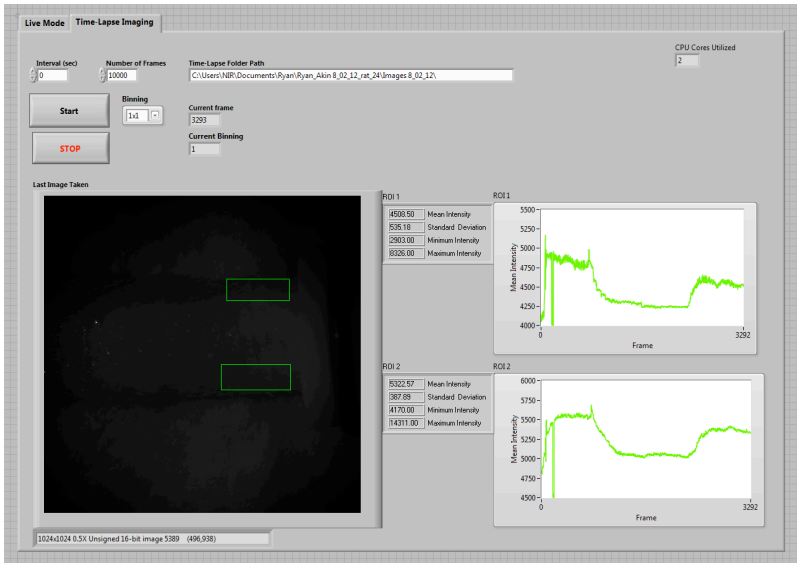

Figure B.9 Rat 8 (Rat 24 – 8/2/12): It appeared from the intensity plot that flow was restored in ROI2 at around 25 mmHg. Flow had definitely been restored in ROI2 at 25 mmHg. These intensity plots were the most definitive to this point. The pressure curve stayed at 22.5 mmHg for twice as long as it should have due to a programming failure, but otherwise this was a great trial.

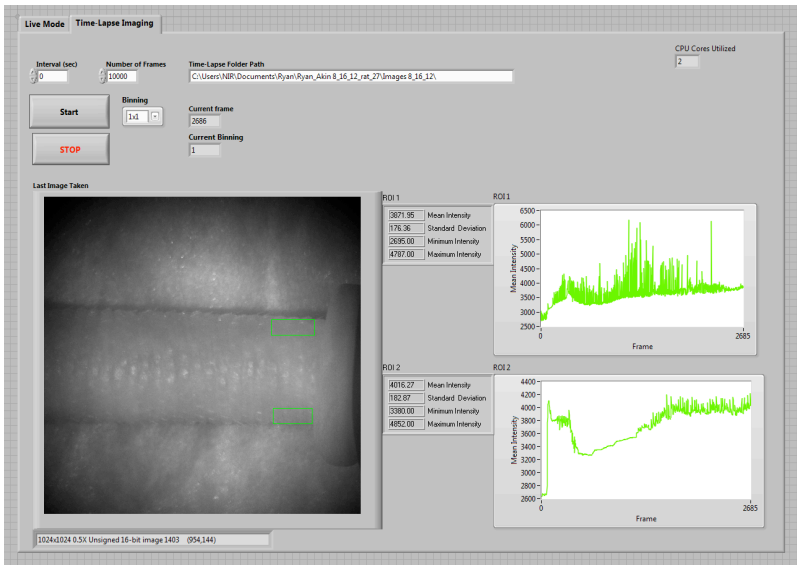

Figure B.10 Rat 9 (Rat 25 – 8/9/12): Great packet flow was observed in ROI1. Poor packet flow was detected in ROI2, but some could be seen. Intensity levels had time to become steady before the pressure cuff was inflated. The shutter malfunctioned some throughout the experiment, which produced the noise in the ROI1 intensity plot. An increase in intensity was observed at 32.5 mmHg and became slightly more visible at 30 mmHg. Flow was seen in ROI1 above 32.5 mmHg.

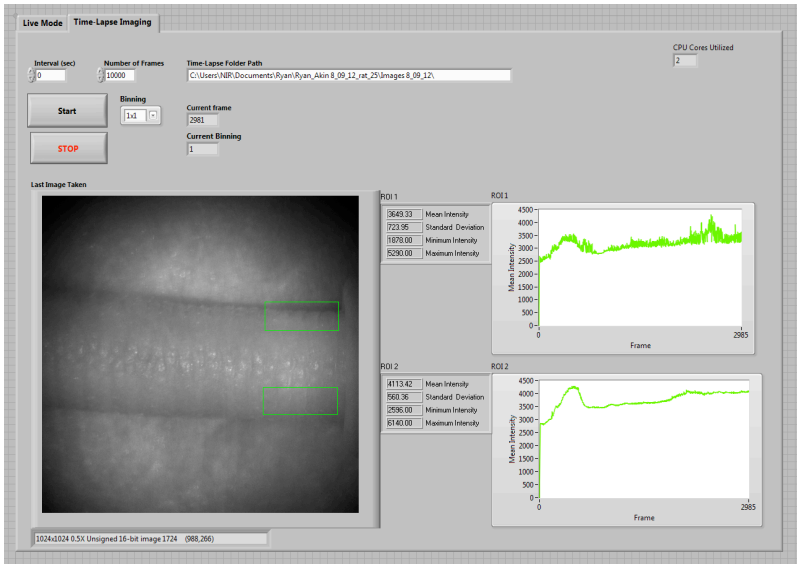

Figure B.11 Rat 10 (Rat 26 – 8/9/12): This trial exhibited the most obvious packet flow in ROI2 of any trial. Not all of the ICG ended up in the vessel during injection because some escaped through the punctured dermis. The shutter of the camera malfunctioned throughout the trial, having a drastic effect on ROI1 intensity. The tail was positioned towards the bottom of the field of view (FOV) to prevent the glitch from having a large effect on the ROI2 intensity. The tail may have moved slightly during the procedure. A large change in intensity in ROI2 was observed through the plot (but not visually) at 40 mmHg. Packet flow was visible in ROI2 at 32.5 mmHg.

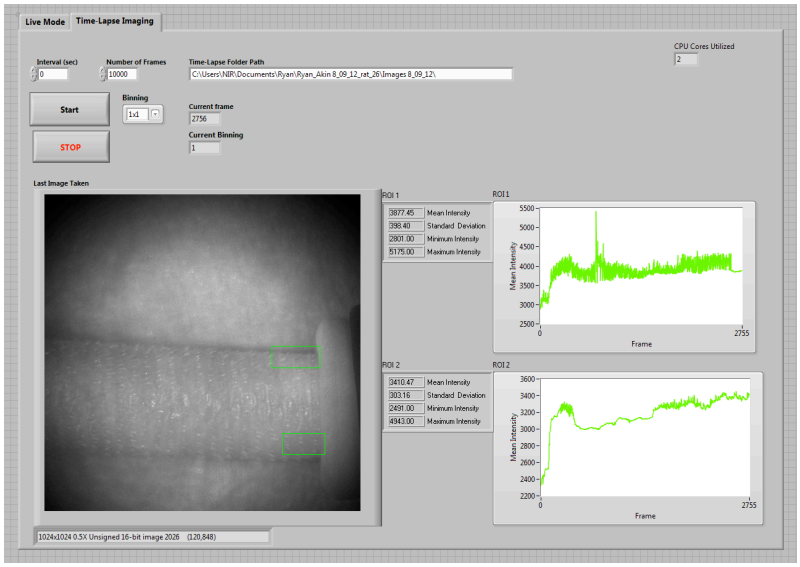

Figure B.12 Rat 11 (Rat 27 – 8/16/12): The shutter issue progressed, rendering ROI1 intensity values useless. The camera was left on for 15-20 minutes before the trial to reduce the glitch, but this did not work as it had at times in the past. Flow was easily observed in ROI2. Inflation of cuff may have adjusted ROIs slightly, so the tail was slightly moved back to align ROIs around frame 428. Intensity continued to rise even though the cuff was inflated and flow could not be visually confirmed. First packets, fast-moving upon return, were seen at 35 mmHg.

APPENDIX C

LABVIEW VISUAL INSTRUMENTS (VI'S) AND CODE

This portion of the Appendix details the National Instrument (NI) LabView Virtual Instrument (VI) that was compiled to control the pressure cuff system. The Block Diagram (BD) is used along with MATLAB script in-line code to acquire, disseminate, and send out information. The Front Panel (FP) is the graphical user interface (GUI) counterpart of the Block Diagram. “Sequences” are executed in series and each Sequence has many nested VIs. The details of this program are described.

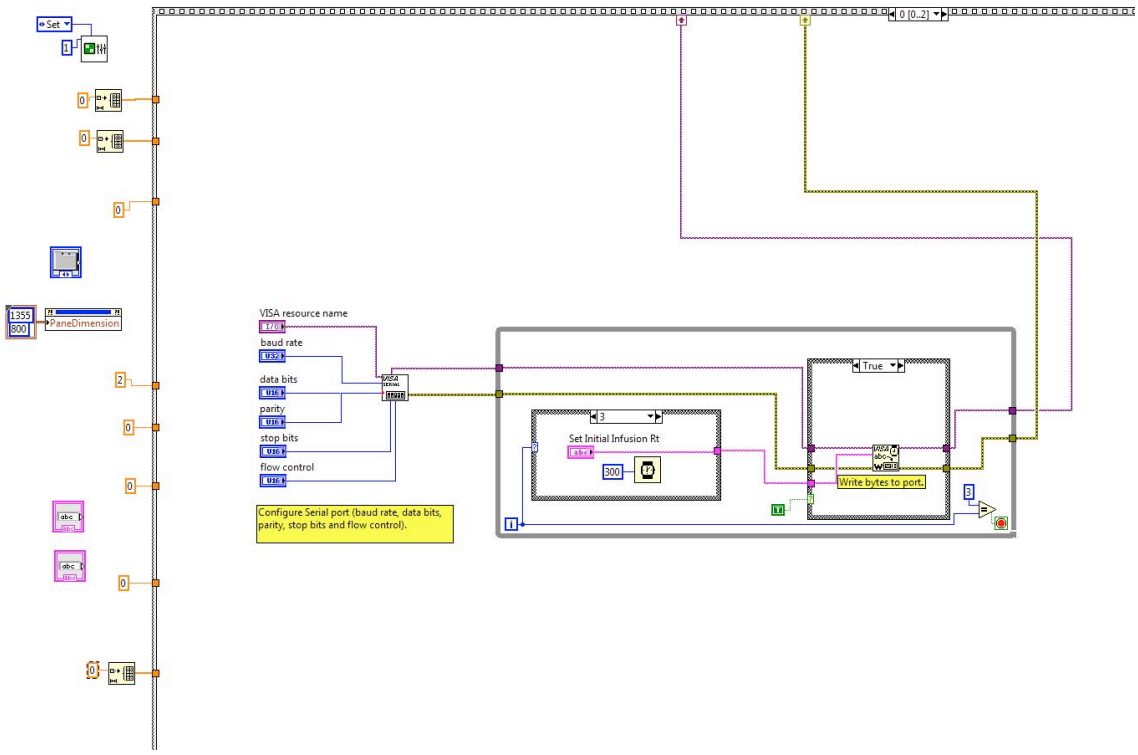

Figure C.1 Sequence 0: This is the beginning of the pressure cuff control system. Its primary purpose is to communicate necessary operational parameters to the syringe pump including VISA resource name (USB Port of the computer), baud rate, number of data bits, the parity, number of stop bits, and a flow control string. Additionally, the portion of the Block Diagram in the Case Structure sends serial commands to enter the syringe diameter, initial syringe infusion rate, and initial syringe refill rate. The later two translate into inflation and deflation rates respectively. Although this image cuts off part of Sequence 0, it includes all of the pertinent Visual Instruments (VIs) before moving to Sequence 1.

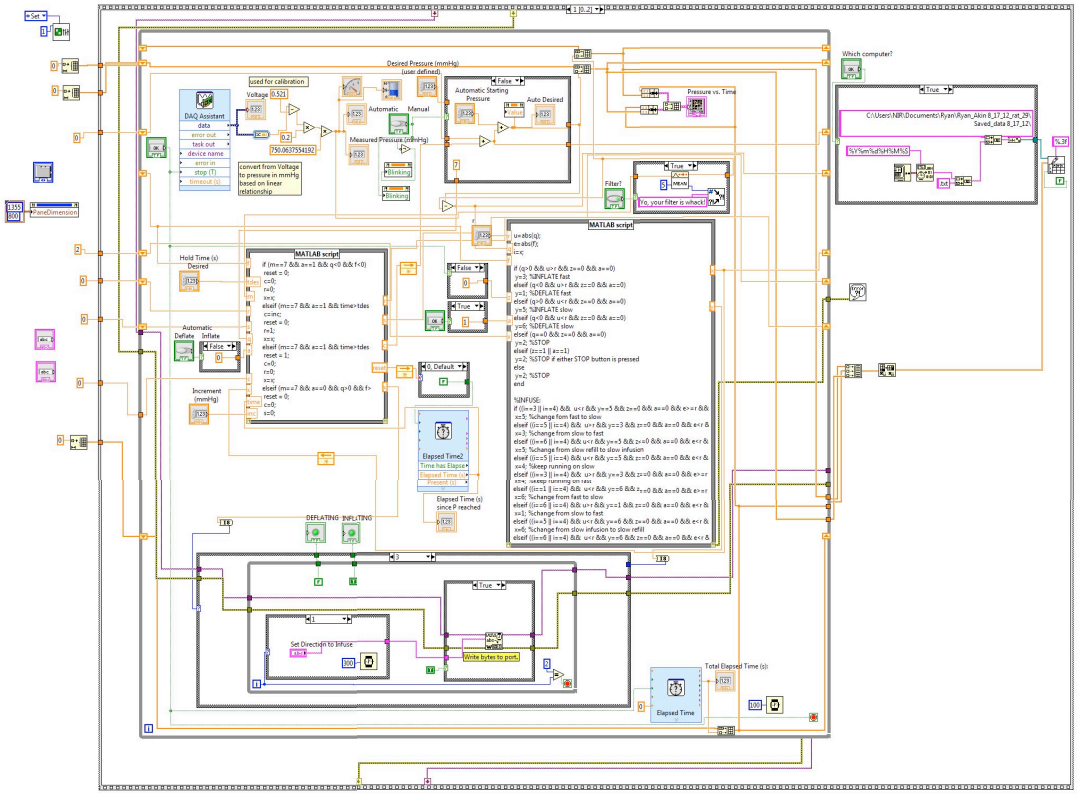

Figure C.2 Sequence 1: This is the "brain" of the pressure cuff control system. It is in this part of the VI that critical decisions are made in terms of commands sent to the syringe pump based on data acquired from the pressure transducer. The top left of the image depicts the voltage acquisition (from the DAQ) and converted into pressure. The top middle is the portion of the VI that allows the user to select either "Manual" or "Automatic" input of desired pressure. The top right shows the filter, graph VI, and VIs used to save data to a file name designated by the user. The MATLAB script on the left is involved in the automation of the desired pressure curve and the MATLAB script on the right is where all decisions are made regarding location and speed of inflation/deflation of the cuff. This information is conveyed to the bottom of the image where it is translated into serial code and sent to the syringe pump. A more detailed description of each of these portions of Sequence 1 is provided in the subsequent pages.

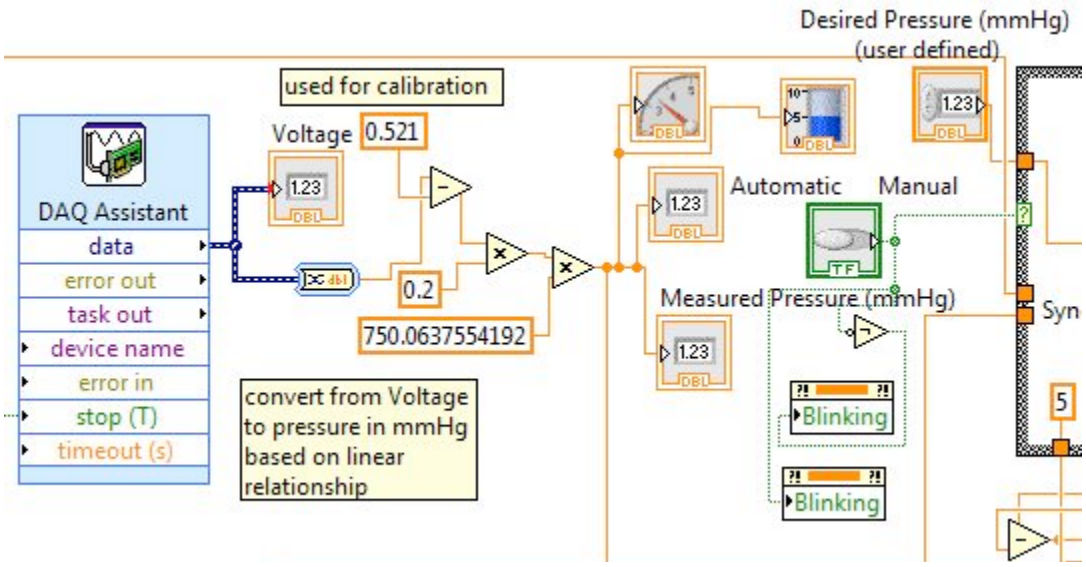

Figure C.3 Voltage Acquisition and Conversion to Pressure: On the left side the DAQ Assistant is responsible for acquiring the voltage signal from the USB6009 at a frequency of 1000 Hz. The value "0.521" was subject to change during intermittent calibration of the pressure transducer throughout the study. This value was used to bring the pressure transducer voltage reading down to zero when the system was open. The "0.2" multiplier was used, because the pressure transducer measurement was between 0 and 5 volts, to provide an overall percentage of the 1 torr max of the pressure transducer. Note, the transducer had a linear relationship between voltage value and pressure reading. Then, the percentage of 1 torr was converted to mmHg using the conversion constant "750.0637554192". This pressure was displayed on the Front Panel numerically and graphically.

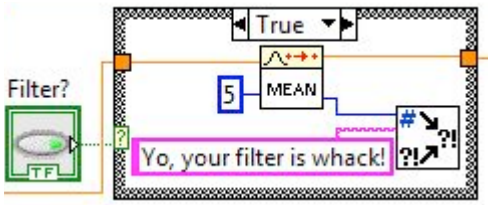

Figure C.4 Filter: The user can select whether or not to filter the actual pressure using a 5 data point Mean Filter. If an error occurs, the message is displayed and the user can troubleshoot the problem.

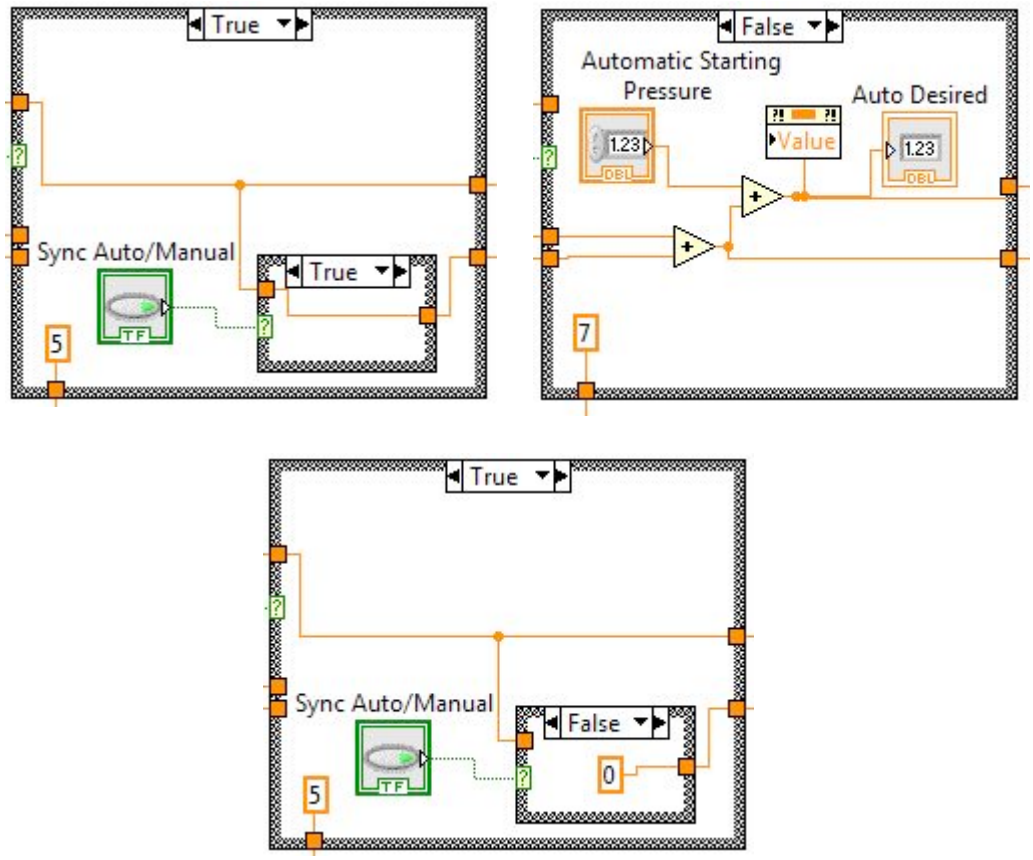

Figure C.5 Manual/Automatic Control Selection: On the left is the Case Structure for Manual Control in which the user inputs a desired pressure which remains until another pressure is typed in. The Sync Auto/Manual Case Structure allows the user to ensure that the desired pressure will not change when switching between Manual/Automatic. The image at the bottom shows the case when the Sync Auto/Manual option is not utilized. On the right is the Case Structure for Automatic Control. It takes inputs from the Automatic MATLAB script on the left in the Block Diagram. The Automatic Starting Pressure can be used to adjust the initial value of the

Automatic MATLAB script: This portion of the program is used to make decisions about when and how to adjust the desired pressure when the user defines the pressure curve to be automatic:

m=7 when the user has chosen Automatic control
m=5 when the user has chosen Manual control
a=0 when the user has chosen to Inflate the cuff
a=1 when the user has chosen to Deflate the cuff
q is the error = desired pressure – actual pressure
f is the error from the previous iteration of the While Loop
time is the elapsed time since the pressure reached the previous desired pressure
tdes is the Hold Time defined by the user
r, s, and c are a dummy variables
reset restarts the Elapsed Time clock when a desired pressure has been reached
x is a variable from the other MATLAB script
inc = the increment of pressure change defined by the user

```
if (m==7 && a==1 && q<0 && f<0)
 reset = 0;
 c=0;
 r=0;
 x=x;
elseif (m==7 && a==1 && time>tdes && r==0)
 c=inc;
 reset = 0;
 r=1;
 x=x;
elseif (m==7 && a==1 && time>tdes && q<0 && f>0)
 reset = 1;
 c=0;
 r=0;
 x=x;
elseif (m==7 && a==0 && q>0 && f>0)
 reset = 0;
 c=0;
 s=0;
 x=x;
elseif (m==7 && a==0 && time>tdes && s==0)
 c=-1*inc;
 reset = 0;
 s=1;
 x=x;
elseif (m==7 && a==0 && time>tdes &&  q>0 && f<0)
 reset = 1;
 c=0;
 s=0;
 x=x;
else
 reset = 0; c=0; x=x;
end
```

Decision MATLAB script: The purpose of this script is to make decisions about which command should be sent to the syringe pump based on several factors including those listed below.

q is the error = desired pressure – actual pressure
f is the error from the previous iteration of the While Loop
u, e, i, y are dummy variables
z = 0 when the user has not stopped the program on the Front Panel
z = 1 when the user has stopped the program on the Front Panel
a = 0 when the user has not stopped the pump on the Front Panel
a = 1 when the user has stopped the pump on the Front Panel
x transfers the output of this script to the portion of the Block Diagram that sends serial commands to the syringe pump via the Automatic MATLAB script

Note: The reason for the "keep running" commands is to eliminate the sending of unnecessary commands to the syringe pump, which require much more time to transmit.

```
u=abs(q);
e=abs(f);
i=x;

if (q>0 && u>r && z==0 && a==0)
 y=3; %INFLATE fast
elseif (q<0 && u>r && z==0 && a==0)
 y=1; %DEFLATE fast
elseif (q>0 && u<r && z==0 && a==0)
 y=5; %INFLATE slow
elseif (q<0 && u<r && z==0 && a==0)
 y=6; %DEFLATE slow
elseif (q==0 && z==0 && a==0)
 y=2; %STOP
elseif (z==1 || a==1)
 y=2; %STOP if either STOP button is pressed
else
 y=2; %STOP
end

%INFUSE/REFILL:
if ((i==3 || i==4) &&  u<r && y==5 && z==0 && a==0 && e>=r && q>=0 && f>=0)
 x=5; %change fom fast to slow
elseif ((i==5 || i==4) &&  u>r && y==3 && z==0 && a==0 && e<r && q>=0 && f>=0)
 x=3; %change from slow to fast
elseif ((i==6 || i==4) && u<r && y==5 && z==0 && a==0 && e<r && q>=0 && f<0)
 x=5; %change from slow refill to slow infusion
elseif ((i==5 || i==4) && u<r && y==5 && z==0 && a==0 && e<r && q>=0 && f>=0)
 x=4; %keep running on slow
elseif ((i==3 || i==4) &&  u>r && y==3 && z==0 && a==0 && e>=r && q>=0 &&f>=0)
```

```
 x=4; %keep running on fast
elseif ((i==1 || i==4) &&  u<r && y==6 && z==0 && a==0 && e>=r && q<0 && f<0)
 x=6; %change from fast to slow
elseif ((i==6 || i==4) && u>r && y==1 && z==0 && a==0 && e<r && q<0 && f<0)
 x=1; %change from slow to fast
elseif ((i==5 || i==4) && u<r && y==6 && z==0 && a==0 && e<r && q<0 && f>=0)
 x=6; %change from slow infusion to slow refill
elseif ((i==6 || i==4) &&  u<r && y==6 && z==0 && a==0 && e<r && q<0 && f<0)
 x=4; %keep running on slow
elseif ((i==1 || i==4) && u>r && y==1 && z==0 && a==0 && e>=r && q<0 && f<0)
 x=4; %keep running on fast
else
 x=y;
end
```

The value of "x" as it comes to the Case Structure at the bottom of the Block Diagram determines the case that is selected. The following will offer an explanation for each of those cases, which correlate to the about Decision MATLAB script.

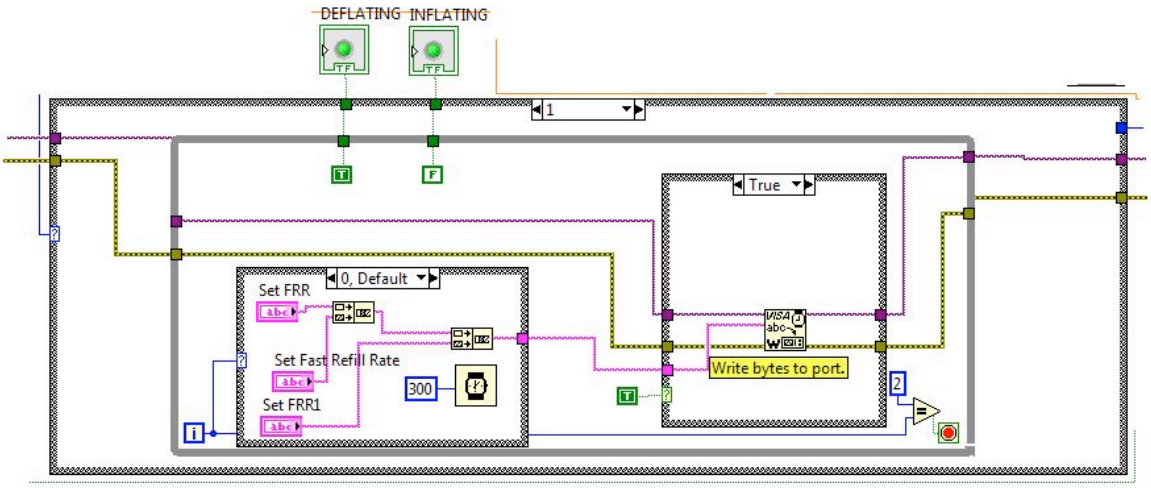

Figure C.6 Case 1.0: Commands are sent to the syringe pump to set the Refill Rate to the Fast Refill Rate indicated by the user in the Front Panel (FP) tab "Serial Commands".

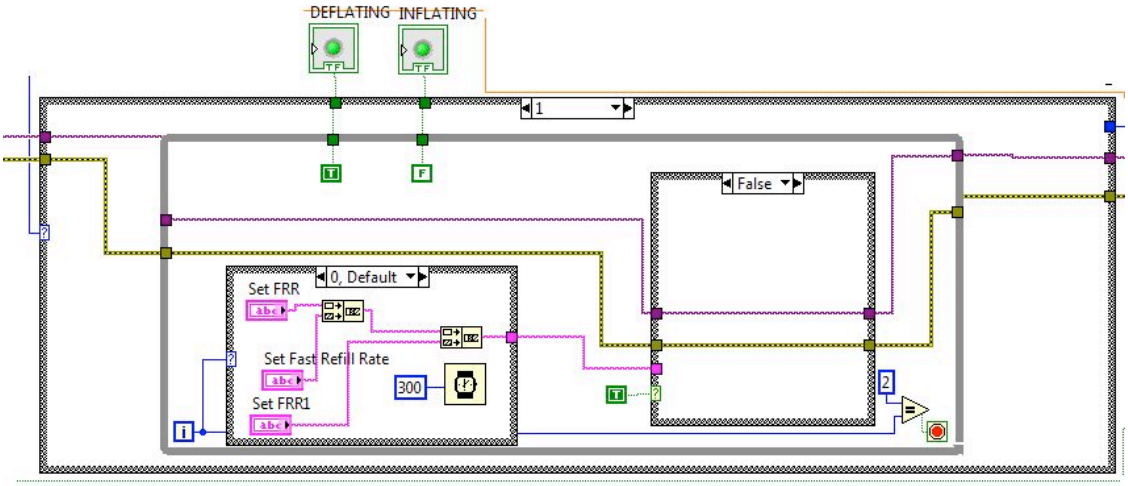

Figure C.7 Case 1.0 False: Commands are not sent to the syringe pump if the nested Case Structure is set to "False"

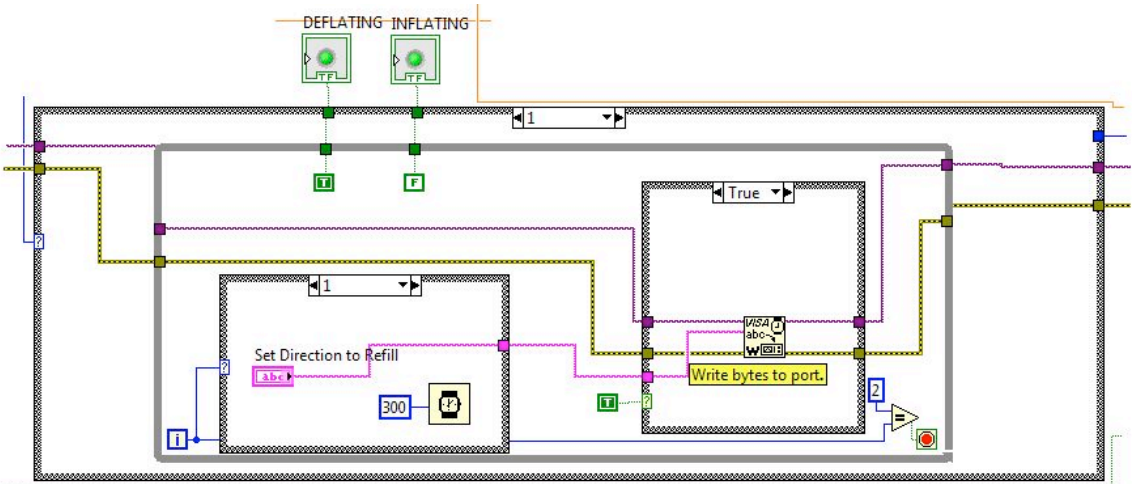

Figure C.8 Case 1.1: Commands are sent to the syringe pump to set the Direction to Refill using the commands indicated by the user in the FP tab "Serial Commands".

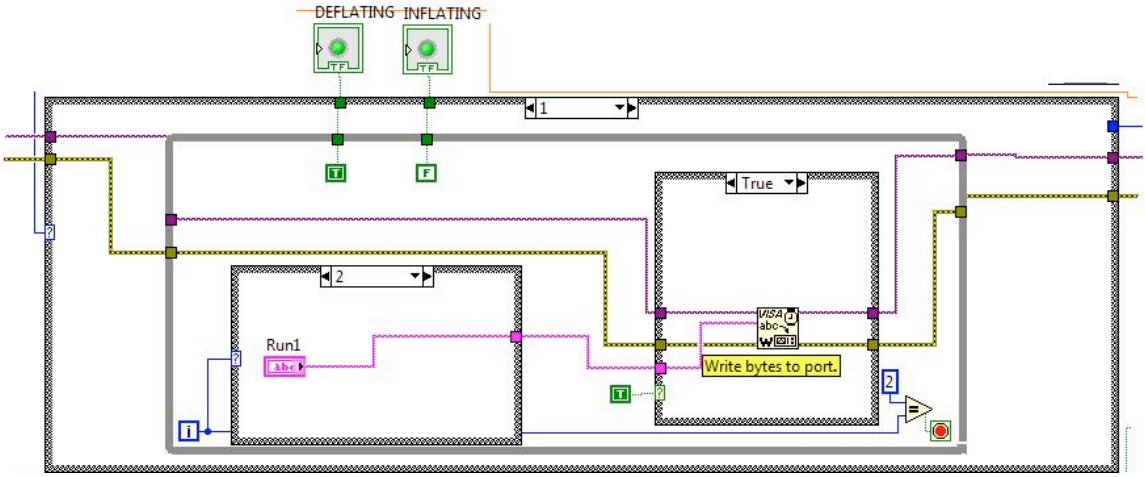

Figure C.9 Case 1.2: Commands are sent to the syringe pump to "Run" it using the commands indicated by the user in the FP tab "Serial Commands".

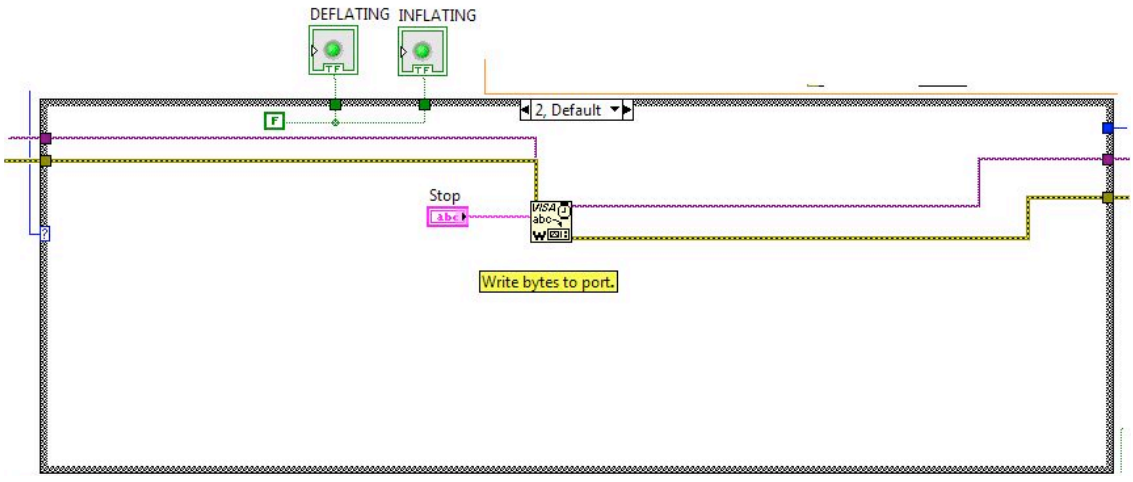

Figure C.10 Case 2: Commands are sent to the syringe pump to "Stop" it using the commands indicated by the user in the FP tab "Serial Commands".

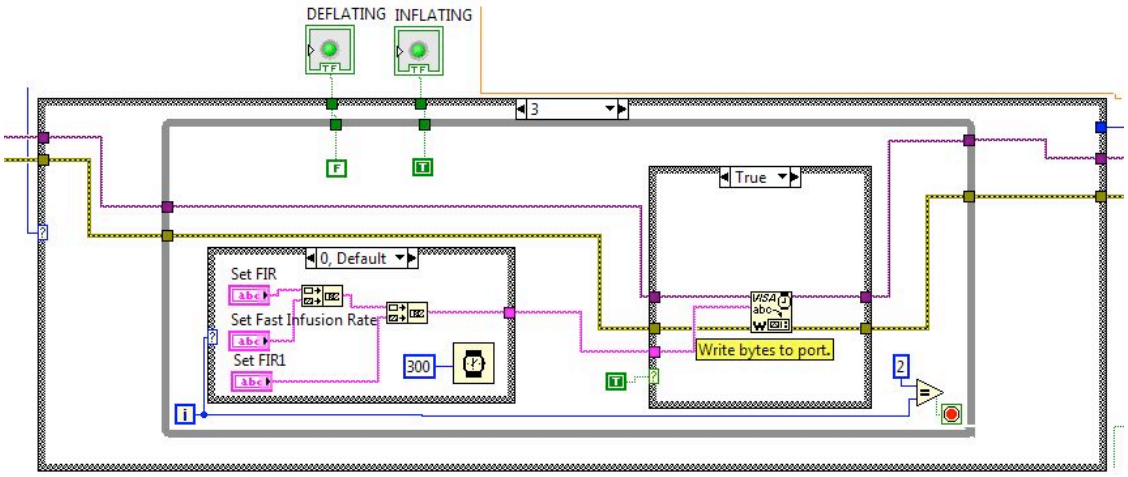

Figure C.11 Case 3.0: Commands are sent to the syringe pump to set the Infusion Rate to the Fast Infusion Rate indicated by the user in the FP tab "Serial Commands".

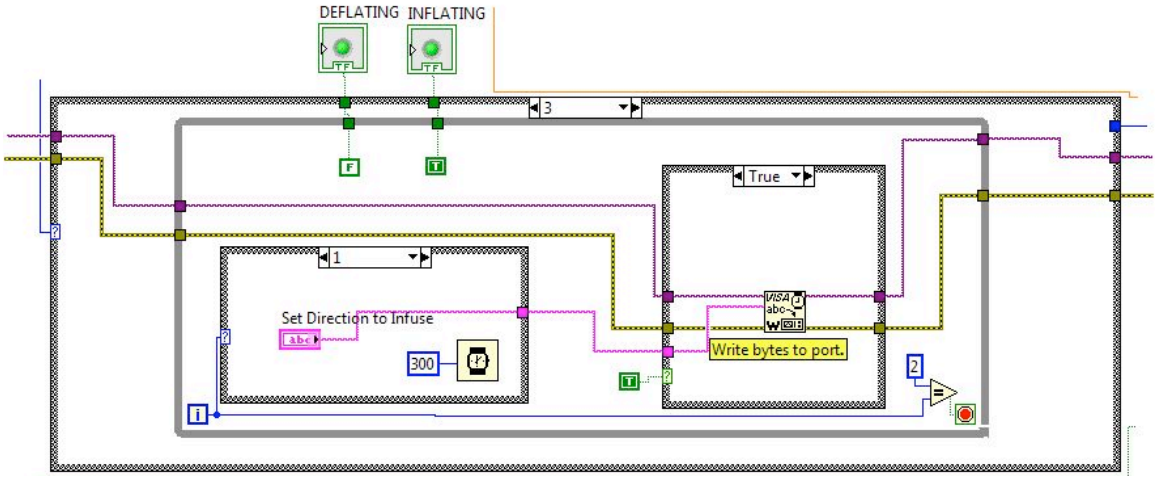

Figure C.12 Case 3.1: Commands are sent to the syringe pump to set the Direction to Infuse using the commands indicated by the user in the FP tab "Serial Commands".

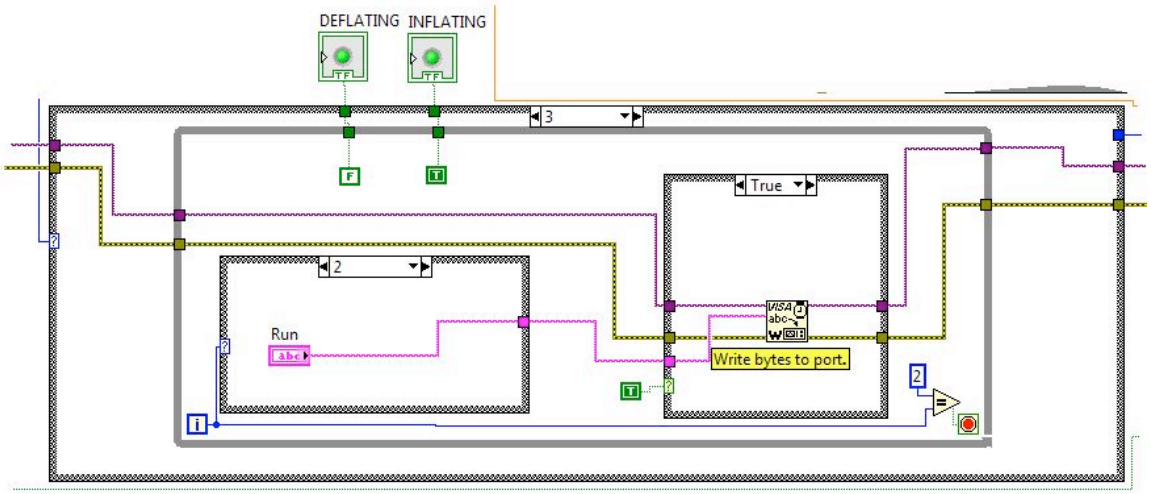

Figure C.13 Case 3.2: Commands are sent to the syringe pump to "Run" it using the commands indicated by the user in the FP tab "Serial Commands".

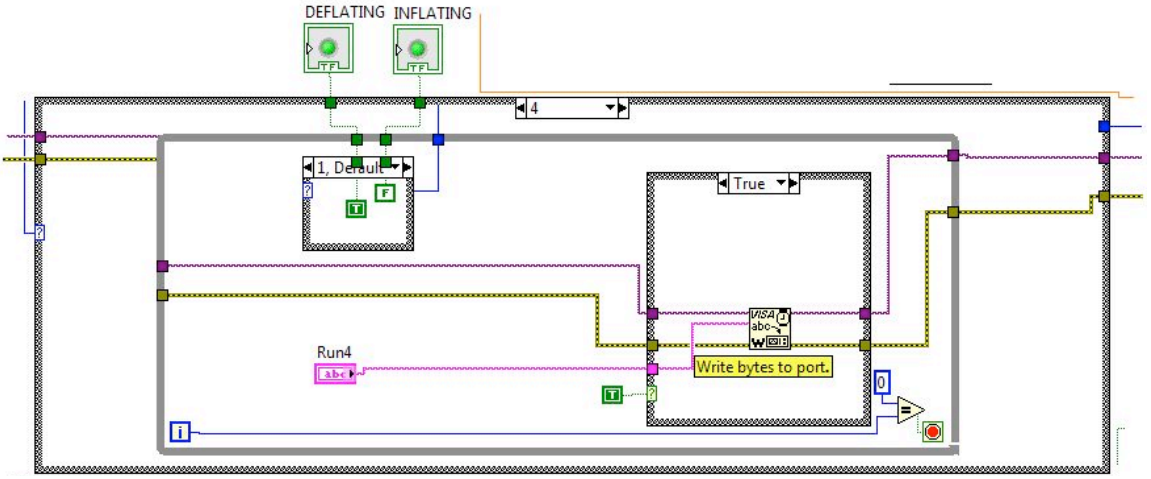

Figure C.14 Case 4: Commands are sent to the syringe pump to "Run" it using the commands indicated by the user in the FP tab "Serial Commands".

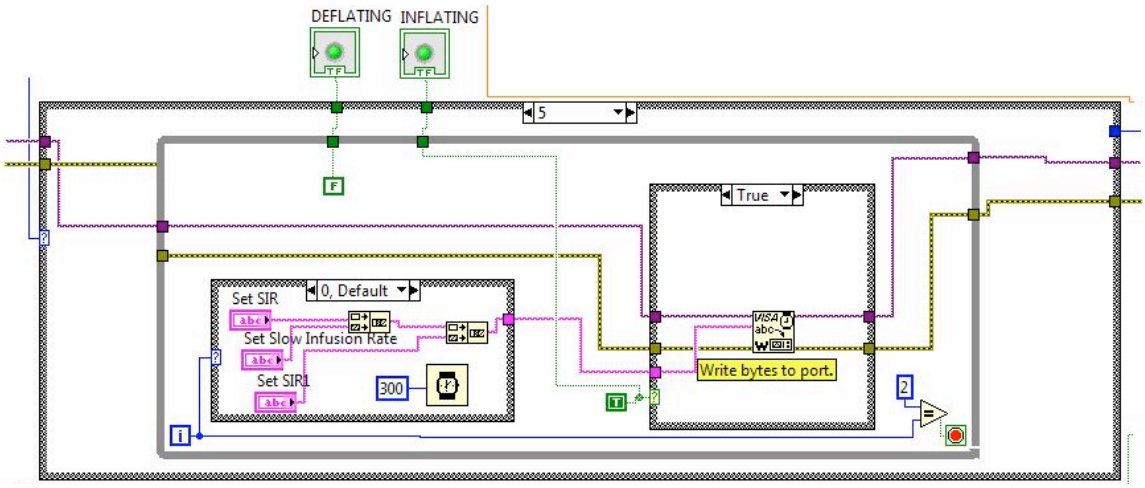

Figure C.15 Case 5.0: Commands are sent to the syringe pump to set the Infusion Rate to the Slow Infusion Rate indicated by the user in the FP tab "Serial Commands".

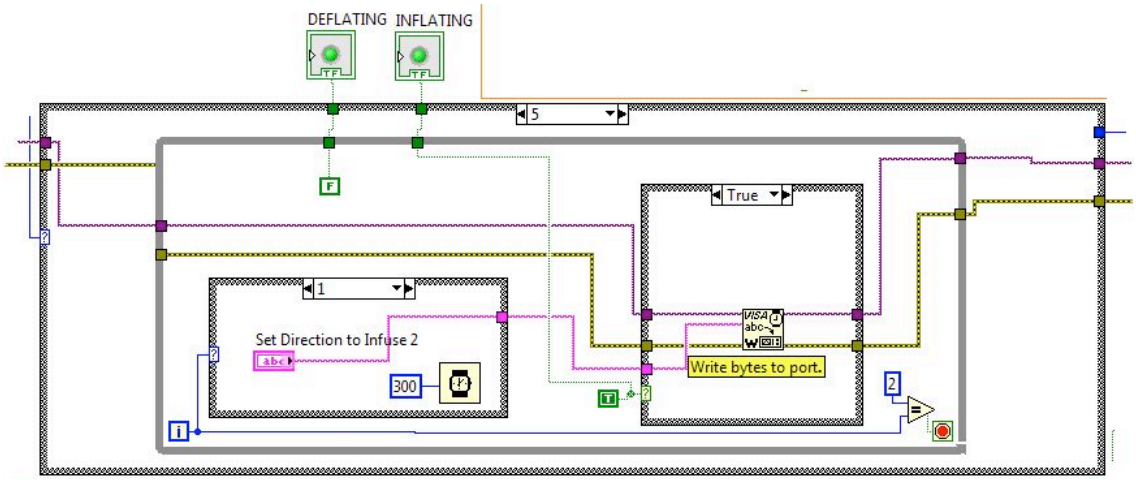

Figure C.16 Case 5.1: Commands are sent to the syringe pump to set the Direction to Infuse using the commands indicated by the user in the FP tab "Serial Commands".

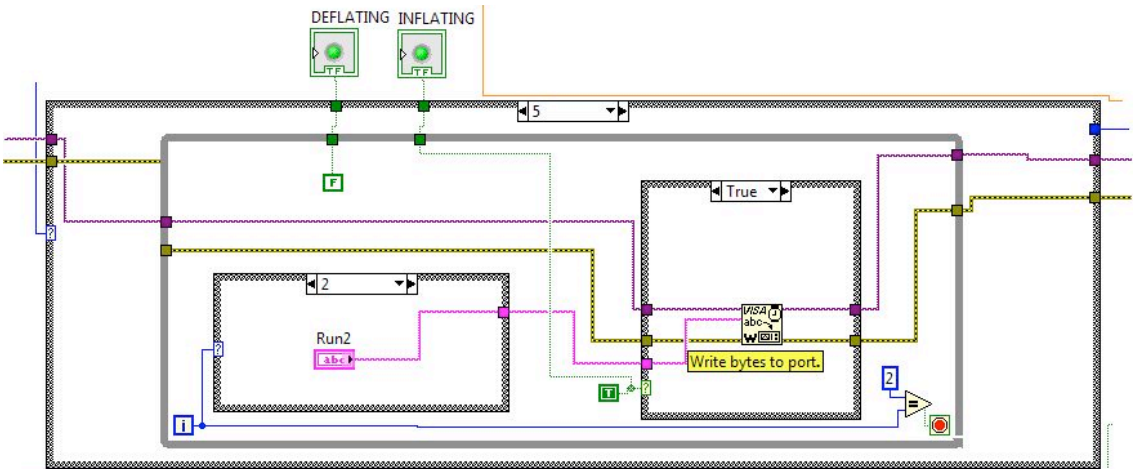

Figure C.17 Case 5.2: Commands are sent to the syringe pump to "Run" it using the commands indicated by the user in the FP tab "Serial Commands".

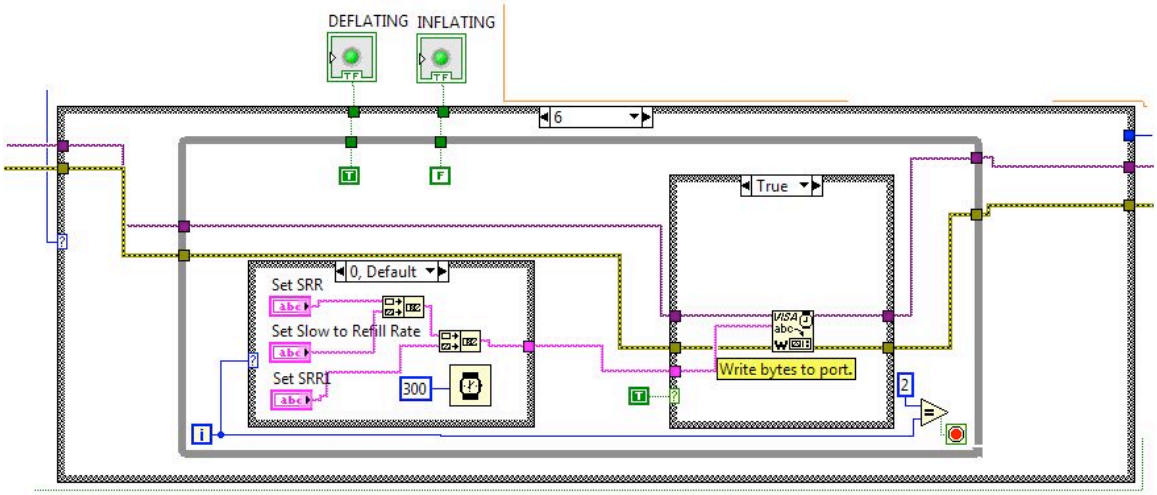

Figure C.18 Case 6.0: Commands are sent to the syringe pump to set the Refill Rate to the Slow Refill Rate indicated by the user in the FP tab "Serial Commands".

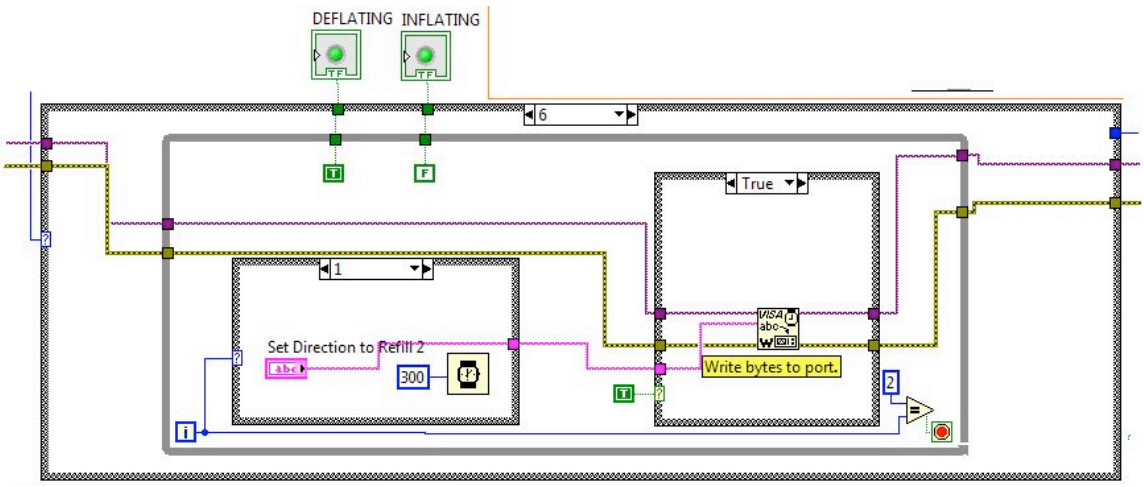

Figure C.19 Case 6.1: Commands are sent to the syringe pump to set the Direction to Refill using the commands indicated by the user in the FP tab "Serial Commands".

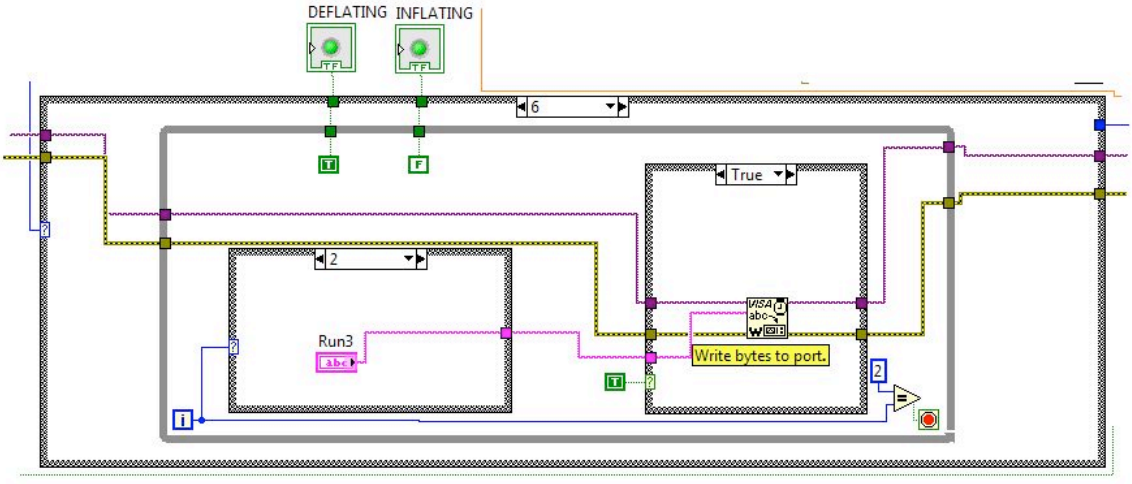

Figure C.20 Case 6.2: Commands are sent to the syringe pump to "Run" it using the commands indicated by the user in the FP tab "Serial Commands".

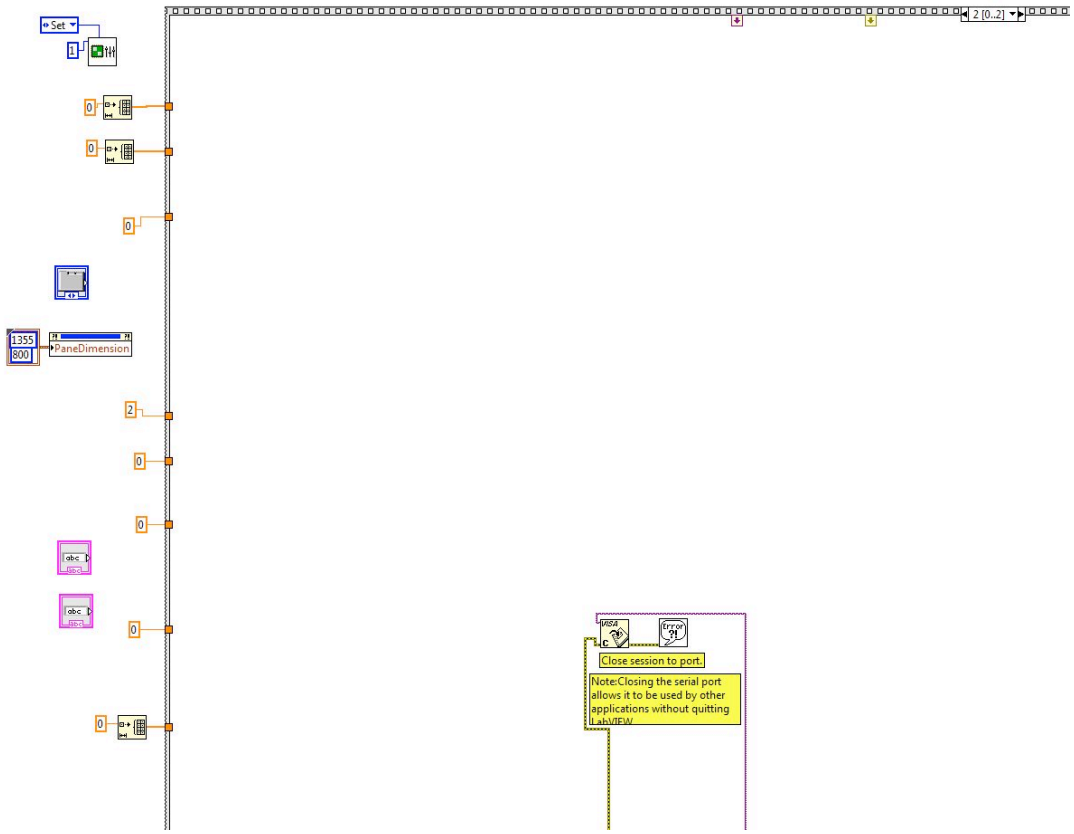

Figure C.21 Sequence 3: This portion of the code is only performed after the user stops the program. It ends communication with the syringe pump so that it can be accessed by another program or manual operation without being interrupted by the Pressure Cuff System Program.

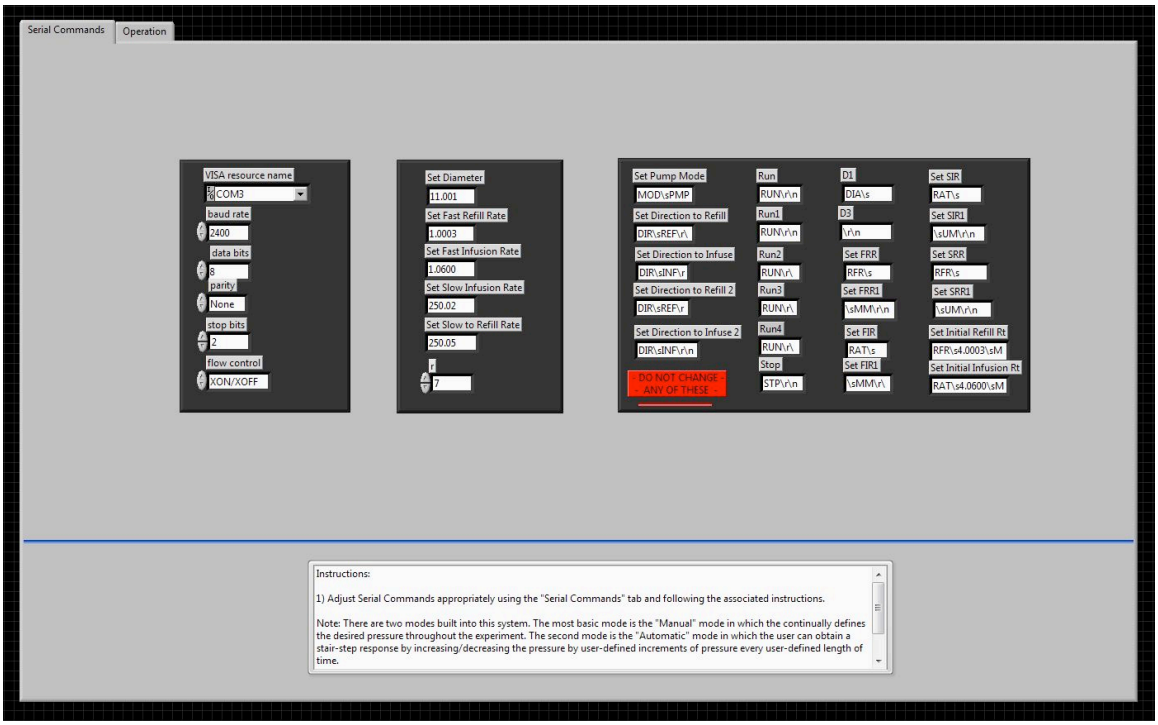

Figure C.22 Serial Commands Tab of Front Panel: Here the user can define the serial commands that are sent to the syringe pump throughout the program. It is recommended that most of these commands should not be altered because they must be formatted very specifically.

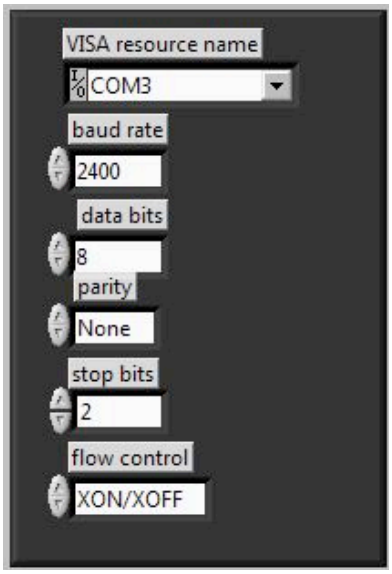

Figure C.23 Syringe Pump Formatting Serial Commands: These commands must match the set-up of the syringe pump for proper communication with it. Although operation would theoretically be faster with a higher baud rate, the syringe pump did not accept commands well at higher baud rates. The COM# is the port of the computer to which the USB cable from the syringe pump is connected.

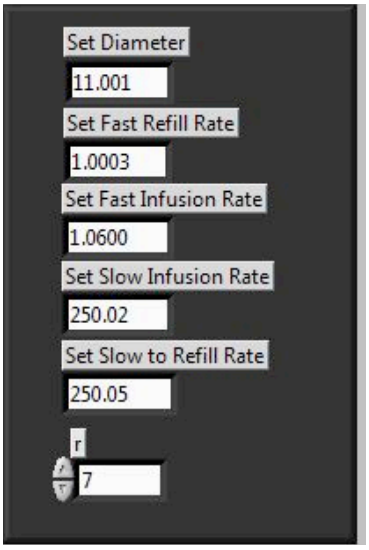

Figure C.24 Numeric Input to Syringe Pump: Aside from the COM# in the previous image and the units in the subsequent image, these are the only serial commands that the user may define preferentially. The diameter must match that of the syringe if the user desires accurate volume flow rates, although they were not used for anything in this study. If Refill/Infusion rates are outside of the operation range the syringe pump will display an error message. The "r" value is the range from the desired pressure value within which the Refill/Infusion Rate changes from Fast to Slow. Units for these values are defined in the Text Input to Syringe Pump portion of the Front Panel.

Figure C.25 Text Input to Syringe Pump: These serial commands are used to set up various parameters for use during execution of the program. These are linked to the same titled icons on the BD. The only text that may need to be altered by a user is the units (UM, MM, etc.) for Refill/Infusion Rates per the Syringe Pump User Manual (Harvard Apparatus – PHD 2000 Syringe Pump Series User Manual – found online).

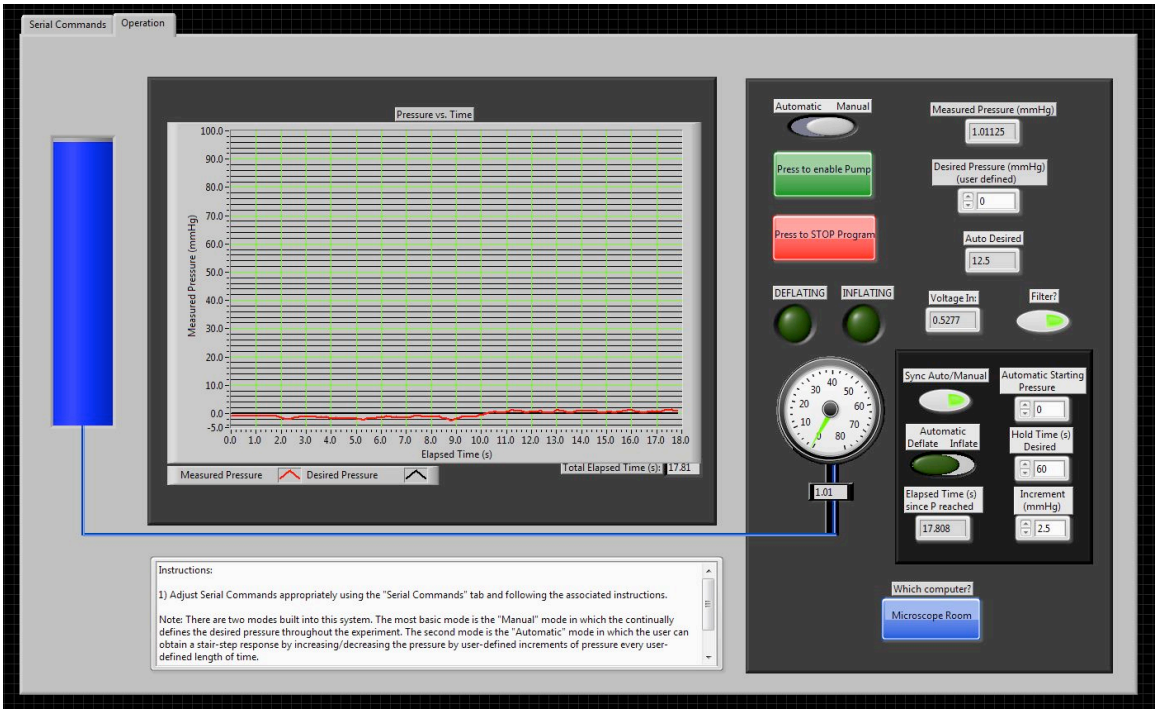

Figure C.26 Operation Tab of Front Panel: This is the primary GUI utilized during experimentation. It has been set up as a user-friendly tool for making real-time adjustments during program execution, while also providing essential indicators depicting feedback from the system. The plot on the left side shows the Desired Pressure and Experimental (Actual) Pressure in mmHg in the pressure cuff as a function of time in seconds. The controls on the right are explained below.

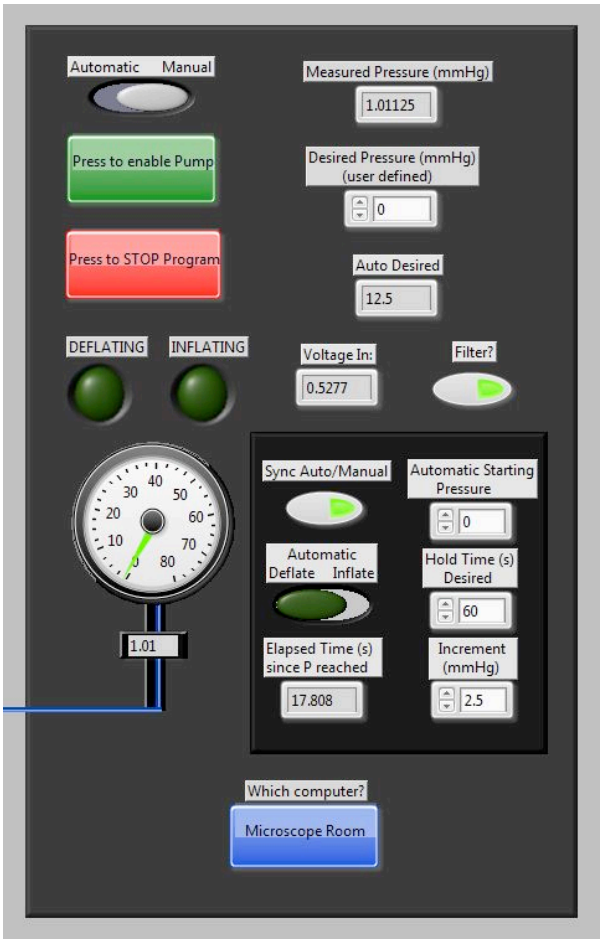

Figure C.27 Operation Tab of Front Panel – Execution Panel: This is the only place in the GUI that the user will need to input information throughout execution of the program. The top stop button (green) allows the user to stop the pump without stopping the program. The bottom stop button (red) allows the user to stop the entire program. If the user does not stop the pump a couple of seconds before stopping the program, then the syringe pump may continue to run. The user can select Automatic or Manual operation via the toggle switch at the top left. If Manual operation is selected, then the user can type in a Desired Pressure on the right side. If the user selects Automatic operation, then the controls at the bottom right will be utilized. The Sync Auto/Manual toggle switch allows the user to sync up the two so the desired pressure will remain unchanged when the Automatic/Manual switch is toggled. The Automatic Deflate/Inflate toggle switch determines the direction of Desired Pressure increments. The Hold Time specifies the amount of time that the desired pressure stays at a specific value after it is reached by the experimental pressure for the first time before it is automatically incremented or decremented. The Increment value specifies how much the Desired Pressure is adjusted due to each adjustment. The user can select between two computers to specify the directory for saving the output text file. The rest of this portion of the FP includes indicators for various measurements throughout the experiment.

APPENDIX D

LOG OF ANESTHESIA ADMINISTERED TO RATS

Table D Log of Anesthesia Administered to Rats. This table shows the weight of each rat and the amount of anesthetic used. The rats used in data collection of the paper in Chapter 2 are highlighted. In initial experiments the DOB of the rats was not recorded because it was not pertinent at the time of the trials.

Date	Weight	Gender	D.O.B.	Anesthetic	Amount Used
4/6/12	380	M	11/11/11	Diazepam/Innovar-Vet	0.19/0.11
5/18/12	180+	M		Diazepam/Innovar-Vet	0.09/0.05
5/24/12?	290	M		Diazepam/Innovar-Vet	0.15/0.09
6/8/12	199.3	F	3/30/12	Diazepam/Innovar-Vet	0.10/0.06
6/11/12	210	F	3/30/12	Diazepam/Innovar-Vet	0.10/0.06
6/14/12	370	F	3/23/12	Diazepam/Innovar-Vet	0.19/0.11
6/14/12	335	F	3/23/12	Diazepam/Innovar-Vet	0.17/0.10
6/27/12	225	F	4/6/12	Diazepam/Innovar-Vet	0.11/0.07
7/2/12	300	M	4/20/12	Diazepam/Innovar-Vet	0.15/0.09
7/2/12	340	M	4/20/12	Diazepam/Innovar-Vet	0.15/0.10
7/12/12	366.9	M	4/20/12	Diazepam/Innovar-Vet	0.18/0.11
7/13/12	335.6	M	4/20/12	Diazepam/Innovar-Vet	0.16/0.09
7/19/12	340	M	4/27/12	Diazepam/Innovar-Vet	0.16/0.10
7/19/12	355	M	4/27/12	Diazepam/Innovar-Vet	0.12/0.07
7/20/12	312.2	M	5/1/12	Diazepam/Innovar-Vet	0.14/0.08
7/20/12	303.6	M	5/1/12	Diazepam/Innovar-Vet	0.15/0.09
7/26/12	250	M	5/25/12	Diazepam/Innovar-Vet	0.13/0.08
7/26/12	243	M	5/25/12	Diazepam/Innovar-Vet	0.12/0.07
7/27/12	246	M	5/25/12	Diazepam/Innovar-Vet	0.13/0.08
7/27/12	250.5	M	5/25/12	Diazepam/Innovar-Vet	0.13/0.08
8/1/12	252.4	M	6/1/12	Diazepam/Innovar-Vet	0.13/0.08
8/1/12	258.9	M	6/1/12	Diazepam/Innovar-Vet	0.13/0.08
8/2/12	292.5	M	6/1/12	Diazepam/Innovar-Vet	0.15/0.09
8/2/12	239.9	M	6/1/12	Diazepam/Innovar-Vet	0.12/0.07
8/9/12	273	M	6/8/12	Diazepam/Innovar-Vet	0.14/0.08
8/9/12	250.8	M	6/8/12	Diazepam/Innovar-Vet	0.13/0.08
8/16/12	263.4	M	6/15/12	Diazepam/Innovar-Vet	0.13/0.08
8/16/12	224	M	6/15/12	Diazepam/Innovar-Vet	0.11/0.07
8/17/12	260	M	6/15/12	Diazepam/Innovar-Vet	0.13/0.08
8/17/12	260	M	6/15/12	Diazepam/Innovar-Vet	0.13/0.08

APPENDIX E

LOG OF BLOOD PRESSURE MEASUREMENTS

Table E Log of Blood Pressure measurements

	Rat 1	Rat 2	Rat 3	Rat 4
Age (days)	75	75	75	75
Weight (g)	350	330	332	330
SBP Pre-GTNO	76.3	87.5	52.3	100
DBP Pre-GTNO	48.7	56.5	25.3	62
SBP Post-GTNO	107	85.6	85	110
DBP Post-GTNO	61.6	49	48	65.6

Notes:

- Rats were anesthetized with Diazepam/InnoVar (both expired). Surgical plane was determined by a toe pinch.
- Pre-GTNO values measured (3 values averaged for each measurement).
- GTNO applied, 20 minutes later Post-GTNO values measured (3 values averaged for each measurement).
- Animal temperature was not maintained for these experiments. All rats are SD male.
- SBP = Systolic Blood Pressure
- DBP = Diastolic Blood Pressure

APPENDIX F

RAT LOG USED FOR DATA ANALYSIS

Table F Rat Log used for Data Analysis - based on output of Matlab code shown in Appendix H.

Rat	Ppump frame - 50	Ppump frame -10	Ppump frame - 20	Ppump frame - Nipper	Ppump frame - Kornuta	Ppump frame - Weiler	Ppump time - 50			Ppump time - 10			Ppump time - 20			Ppump time - Nipper			Ppump time - Kornuta			Ppump time - Weiler			End Time		
17	1785	1589	1618	2000	1350	1560	14	42	19	14	39	3	14	39	32	14	45	54	14	35	4	14	38	34	14	57	54
18	1718	1480	1528	1850	1470	1450	16	26	50	16	22	52	16	23	40	16	29	2	16	22	42	16	22	22	16	43	48
19	2639	2229	2286	2560	1280	2240	15	48	57	15	42	7	15	43	4	15	47	39	15	26	18	15	42	18	15	55	2
20	1971	1210	1689	2135	1865	1850	17	3	33	16	50	52	16	58	51	17	6	17	17	1	47	17	1	32	17	13	26
21	1882	1740	1791	2100	1755	1720	15	25	56	15	23	34	15	24	25	15	29	34	15	23	49	15	23	14	15	39	50
22	2575	2295	2523	2590	795	2525	16	45	29	16	40	49	16	44	37	16	45	44	16	15	49	16	44	39	16	52	51
23	1924	901	1343	2495	1605	1595	15	11	32	14	54	29	15	1	51	15	21	3	15	6	13	15	6	3	15	28	40
24	2468	2374	2418	2670	2305	2295	16	36	31	16	34	57	16	35	41	16	39	53	16	33	48	16	33	38	16	50	17
25	1881	981	1195	2100	1760	1695	12	55	40	12	40	40	12	44	14	12	59	19	12	53	39	12	52	34	13	14	2
26	1582	1473	1481	1940	1450	1450	15	22	29	15	20	40	15	20	48	15	28	27	15	20	17	15	20	17	15	42	4
27	1434	1214	1234	1590	1200	1205	10	44	24	10	40	44	10	41	4	10	47	0	10	40	30	10	40	35	11	5	18

"Ppump frame" and "Packet Resume frame" refer to the times of the frames, during image acquisition, at which each occurred as determined by the Matlab code shown in Appendix H.
"Ppump time" and "Packet Resume time" refer to the times coinciding to the "Ppump frame" and "Packet Resume frame" respectively. The 3 columns are in units of "hours", "minutes", and "seconds".
"End Time" refers to the time when the image acquisition was terminated. The 3 columns are in units of "hours", "minutes", and "seconds".
"Last Pressure time" refers to the total amount of seconds the pressure curve was executed before termination.
"Ppump time" and "Packet Resume time" refer to the times (in seconds), during execution of the pressure curve, at which each occurred.
"Ppump" and "Packet Resume" refer to the pressures (in mmHg) corresponding to the "Ppump time" and "Packet time" during the pressure curve execution respectively.
The blank cells represent the trials for which restoration of packet flow could not be detected or determined using the automated Matlab script.
The colored cells represent the rats to which the GTNO ointment was applied.

Table F (Continued) Rat Log used for Data Analysis - based on output of Matlab code shown in Appendix H.

Rat	Ppump seconds from end - 50	Ppump seconds from end - 10	Ppump seconds from end - 20	Ppump seconds from end - Nipper	Ppump seconds from end - Kornuta	Ppump seconds from end - Weiler	Last Pressure time	Ppump time - 50	Ppump time - 10	Ppump time - 20	Ppump time - Nipper	Ppump time - Kornuta	Ppump time - Weiler	Ppump - 50	Ppump - 10	Ppump - 20	Ppump - Nipper	Ppump - Kornuta	Ppump - Weiler	Average (Nipper, Kornuta, Weiler)
17	935	1131	1102	720	1370	1160	2487	1552	1356	1385	1767	1117	1327	27.31	34.57	32.738	19.283	42.524	35.338	32.3816667
18	1018	1256	1208	886	1266	1286	2502	1484	1246	1294	1616	1236	1216	32.127	40.15	37.708	27.616	39.313	40.766	35.8983333
19	365	775	718	443	1724	764	2492	2127	1717	1774	2049	768	1728	7.204	22.42	20.43	10.185	55.062	21.729	28.992
20	593	1354	875	429	699	714	2457	1864	1103	1582	2028	1758	1743	14.619	42.22	24.405	9.803	19.742	19.895	16.48
21	834	976	925	616	961	996	2413	1579	1437	1488	1797	1452	1417	27.31	31.82	29.604	19.13	29.527	32.815	27.1573333
22	442	722	494	427	2222	492	2615	2173	1893	2121	2188	393	2123	7.739	14.77	7.739	5.445	79.985	7.892	31.1073333
23	1028	2051	1609	457	1347	1357	2449	1421	398	840	1992	1102	1092	31.897	79.53	50.093	10.109	41.683	42.524	31.4386667
24	826	920	876	624	989	999	2561	1735	1641	1685	1937	1572	1562	18.366	24.71	22.647	14.467	26.852	27.157	22.8253333
25	1102	2002	1788	883	1223	1288	2479	1377	477	691	1596	1256	1191	34.497	80.06	66.147	24.558	37.631	40.001	34.0633333
26	1175	1284	1276	817	1307	1307	2394	1219	1110	1118	1577	1087	1087	42.218	41.68	39.313	24.864	42.295	42.295	36.4846667
27	1254	1474	1454	1098	1488	1483	2386	1132	912	932	1288	898	903	44.97	47.95	47.417	35.032	47.34	47.035	43.1356667

"Ppump frame" and "Packet Resume frame" refer to the times of the frames, during image acquisition, at which each occurred as determined by the Matlab code shown in Appendix H.
"Ppump time" and "Packet Resume time" refer to the times coinciding to the "Ppump frame" and "Packet Resume frame" respectively. The 3 columns are in units of "hours", "minutes", and "seconds".
"End Time" refers to the time when the image acquisition was terminated. The 3 columns are in units of "hours", "minutes", and "seconds".
"Last Pressure time" refers to the total amount of seconds the pressure curve was executed before termination.
"Ppump time" and "Packet Resume time" refer to the times (in seconds), during execution of the pressure curve, at which each occurred.
"Ppump" and "Packet Resume" refer to the pressures (in mmHg) corresponding to the "Ppump time" and "Packet time" during the pressure curve execution respectively.
The blank cells represent the trials for which restoration of packet flow could not be detected or determined using the automated Matlab script.
The colored cells represent the rats to which the GTNO ointment was applied.

APPENDIX G

RESULTS DATA

Table G Results Data. Results data from Table F in Appendix F. Each Pumping Pressure and Packet Restoration value corresponds to one respective rat trial. Values are in mmHg.

	Control				
	10%	**20%**	**50%**	**LLBB Avg**	**Packet Restore**
	34.57	32.74	27.31	32.38	20.12
	40.15	37.71	32.13	35.90	29.76
	80.06	66.15	34.50	34.06	44.51
	41.68	39.31	42.22	36.48	46.88
	47.95	47.42	44.97	43.14	
Avg:	**49**	**45**	**36**	**36**	**35**
Std Dev:	18.07	13.12	7.27	4.10	12.65

	Treatment				
	22.42	20.43	7.20	28.99	10.19
	42.22	24.41	14.62	16.48	10.11
	31.82	29.60	27.31	27.16	24.86
	14.77	7.74	7.74	31.11	7.74
	79.53	50.09	31.90	31.44	21.73
	24.71	22.65	18.37	22.83	
Avg:	**36**	**26**	**18**	**26**	**15**
Std Dev:	23.29	13.94	10.13	5.76	7.78

Significance:	0.3371	0.0476	0.0081	0.0098	0.0202

APPENDIX H

DATA ANALYSIS CODE – COURTESY OF DR. J. BRANDON DIXON

The following Matlab code was used to determine the Pumping Pressure and Packet Restoration Pressure from the associated intensity plots for each trial. Dr. J. Brandon Dixon wrote this code.

```
clear;
dirOutput = dir('*.txt');
files = {dirOutput(:).name}';

for x=1:(length(files)/2)
    data(x).pressures=importdata(sprintf('%s',files{2*x-
    1}),'\t');

data(x).intensities=importdata(sprintf('%s',files{2*x}),'\t');
end

for n=1:uint8(length(files)/2)
    clear temp temp2 temp3 temp4 temp5 temp6 int2 remnoise
    intensity remnoise2 freqcurve freqmin freqthresh areaslist
    intensity=data(n).intensities.data(:,2);
    remnoise=(((smooth(diff(intensity)>50,20)>0)+(smooth(diff(int
    ensity)<-50,20)>0))==2);
    remnoise=[remnoise; 0];
    remnoise2=remnoise.*medfilt1(intensity,20);
    intensity=(intensity.*not(remnoise)+remnoise2);
    %intensity=smooth(intensity,3);


    int2=(intensity-smooth(intensity,100));
    int2=medfilt1(int2,5);
    for x=650:(length(intensity)-100)
       temp=abs(fft(int2(x:(x+99))));
       temp2(x-649)=mean(temp(3:25));
    end


    freqcurve=smooth(temp2,20);
    [freqmin, minloc]=min(freqcurve);
    temp4=zeros(minloc,1)+1;
    temp5=zeros(length(temp2)-minloc,1);
    temp6=[temp4' temp5']';
    freqthresh=freqmin+(max(freqcurve(1000:length(freqcurve))-
    freqmin)*.5);

    temp3=bwlabel(((smooth(temp2,20))<freqthresh));
    picareas=regionprops(temp3, 'Area');
    for x=1:length(picareas)
        areaslist(x)=picareas(x).Area;
```

```
    end
    [Y,I]=max(areaslist);
    temp2=diff((temp3==I));
    [Y,I2]=min(temp2);
    packetresume(n)=I2+700;


    smoothint=smooth(intensity,20);
    Imin=minloc+659;
    packetvar(n)=var(data(n).intensities.data((packetresume(n)-
    25):(packetresume(n)+25),2));
    refvar(n)=var(data(n).intensities.data((Imin-50):Imin,2));
    packetresume.*((packetvar./refvar)>2)


    minint=smoothint(Imin);
    [maxint,Imax]=max(smoothint(Imin:length(smoothint)));
    thresh=minint+(maxint-minint)*.5;
    temp=find(smoothint(Imin:length(smoothint))>thresh);
    ppump(n)=temp(1)+Imin


end


% % I just copy and paste this code into the command window to
back out
% the actual pressures from the data file
```